

The University of New South Wales
Faculty of Science
School of Materials Science & Engineering

Titanium Surface Modification by Oxidation for Biomedical Application

A Thesis

by

Hasan Z. Abdullah

Submitted in Partial Fulfilment of the
Requirements for the Degree
of
Doctor of Philosophy
in
Materials Science and Engineering

February 2010

ABSTRACT

Surface modification is a process that is applied to the surfaces of titanium substrates in order to improve the biocompatibility after implanting in the body. Two methods were used in the present work: Anodisation and gel oxidation. Anodisation was performed at room temperature in strong mineral acids (sulphuric acid (H_2SO_4) and phosphoric acid (H_3PO_4)), an oxidising agent (hydrogen peroxide (H_2O_2)), mixed solutions of the preceding three, and a weak organic acid mixture (β -glycerophosphate + calcium acetate). The parameters used in anodisation were: Concentrations of the electrolytes, applied voltage, current density, and anodisation time. Gel oxidation was carried out by soaking titanium substrates in sodium hydroxide (NaOH) aqueous solutions at different concentrations (0.5 M, 1.0 M, 5.0 M, and 10.0 M) at 60°C for 24 h, followed by oxidation at 400° , 600° , and 800°C for 1 h.

Conceptual models representing changes in the microstructure as a function of the experimental parameters were developed using the anodisation data. The relevant parameters were: Applied voltage, current density, acid concentration, and anodisation time:

- The model for anodisation using the strong acid (H_2SO_4) illustrates the growth rate of the film, identification of the threshold for the establishment of a consistent microstructure, and prediction of the properties of the film.
- For the oxidising agent (H_2O_2), two models were developed: Current-control and voltage-control, the applicability of which depends on the scale of the current density (high or low, respectively). These models are interpreted in terms of the coherency/incoherency of the corrosion gel, arcing, and porosity.
- The model for the strongest acid (H_3PO_4) is similar to that of H_2O_2 in current-control mode, although this system showed the greatest intensity of arcing and consequent pore size.
- Anodisation in mixed solutions uses Ohm's law to explain four stages of film growth in current-control mode. These stages describe the thickness of the gel, its recrystallisation, and the achievement of a consistent microstructure.

- Anodisation in weaker organic acids allows the most detailed examination of the anodisation process. Both current density and voltage as a function time reveal the nature of the process in six stages: (1) instrumental response, (2 and 3) gel thickening, (4) transformation of the amorphous gel to amorphous titania, (5) recrystallisation of the amorphous titania, and (6) subsurface pore generation upon establishment of a consistent microstructure.

Gel oxidation was done at low and high NaOH concentrations followed by oxidation. Three models were developed to represent the gel oxidation process: (1) Low concentration, (0.5 M and 1.0 M NaOH), (2) Medium concentration (5.0 M NaOH), and (3) high concentration (10.0 M NaOH). For the low concentrations with increasing temperature, the model involves: (1) amorphous sodium titanate forms over a layer of amorphous anatase and (2) a dense layer of rutile forms. For the high concentrations with increasing temperature, the model involves: (1) amorphous sodium titanate forms over a layer of amorphous anatase, (2) a dense layer of anatase forms and raises up the existing porous anatase layer, and (3) the dense and porous anatase layers transform to dense and porous rutile layers, respectively. The main difference between the two is the retention of crystalline sodium titanate in the higher NaOH concentration.

Anodised and gel oxidised samples subsequently were soaked in simulated body fluid in order to study the precipitation of hydroxyapatite in the absence and presence of long UV irradiation, which has not been investigated before. With the anodised surfaces, the porous and rough titania coating facilitated both the precipitation of hydroxyapatite and the attachment of bone-like cells. UV irradiation showed greatly enhanced hydroxyapatite precipitation, which is attributed to its photocatalytic properties. With the gel oxidised surfaces, the greatest amount of hydroxyapatite precipitation occurred with the presence of both anatase and amorphous sodium titanate. Rutile suppressed precipitation.

TABLE OF CONTENTS

| | Page |
|--|-------|
| CERTIFICATE OF ORIGINALITY | ii |
| ACKNOWLEDGEMENTS | iii |
| ABSTRACT | iv |
| TABLE OF CONTENTS | vi |
| LIST OF FIGURES | xiii |
| LIST OF TABLE | xxv |
| LIST OF APPENDICES | xxix |
| LIST OF PUBLICATIONS | xxxix |
| | |
| CHAPTER 1: INTRODUCTION | 1-1 |
| | |
| CHAPTER 2: LITERATURE SURVEY | 2-1 |
| 2.1 Titanium Dioxide (TiO₂) | 2-1 |
| 2.1.1 Uses | 2-1 |
| 2.1.1.1 General | 2-1 |
| 2.1.1.2 Photocatalytic | 2-1 |
| 2.1.1.3 Biomedical Applications | 2-4 |
| 2.1.2 Crystal Structure and Phase Transformation | 2-4 |
| 2.1.2.1 Anatase | 2-6 |
| 2.1.2.2 Rutile | 2-7 |
| 2.1.2.3 Brookite | 2-8 |
| 2.1.3 Thermodynamics and Phase Equilibrium | 2-9 |
| 2.1.4 Properties of TiO ₂ | 2-11 |
| 2.1.4.1 Physical Properties | 2-12 |
| 2.1.4.2 Chemical Properties | 2-14 |
| 2.1.4.3 Optical Properties | 2-15 |
| 2.1.4.4 Photocatalytic Properties | 2-18 |
| | |
| 2.2 Colour Properties of Titanium and TiO₂ | 2-20 |
| 2.2.1 Colour System | 2-20 |
| 2.2.2 RGB-Based Colour Space | 2-21 |

| | | |
|------------|--|------|
| 2.2.3 | HSV and HLS Colour Space | 2-22 |
| 2.2.4 | Colour Measurement | 2-24 |
| 2.2.5 | Titanium and TiO ₂ Colour | 2-26 |
| 2.3 | Titanium and Titanium Alloys | 2-26 |
| 2.3.1 | Biomedical Applications | 2-29 |
| 2.3.2 | Other Applications | 2-32 |
| 2.4 | Tests to Determine Biocompatibility of Titanium | 2-32 |
| 2.4.1 | <i>In Vitro</i> Screening | 2-32 |
| 2.4.1.1 | Cytotoxicity Testing | 2-32 |
| 2.4.1.2 | Bioactivity (Simulated Body Fluid, SBF) | 2-34 |
| 2.4.1.3 | Titanium in Simulated Body Fluid (SBF) | 2-34 |
| 2.4.2 | Biological Test (Cell Culture) | 2-36 |
| 2.4.2.1 | Saos 2 Cell | 2-36 |
| 2.4.2.2 | Morphology of Cells | 2-37 |
| 2.4.2.3 | Cell Response on Titanium Surfaces (Anodic Oxidation, Chemical Treatment) | 2-37 |
| 2.4.3 | <i>In Vivo</i> Tests | 2-39 |
| 2.5 | Method of TiO₂ Fabrication | 2-40 |
| 2.6 | Surface Chemistry of Titanium and Titanium Alloys | 2-41 |
| 2.7 | Film Processing Techniques | 2-43 |
| 2.8 | Electrochemical Treatment (Anodic Oxidation) | 2-43 |
| 2.8.1 | Breakdown Voltage, Voltage and Current | 2-45 |
| 2.8.2 | Anodic Oxidation of Titanium in Sulphuric Acid (H ₂ SO ₄) | 2-46 |
| 2.8.3 | Anodic Oxidation of Titanium in Hydrogen Peroxide (H ₂ O ₂) | 2-48 |
| 2.8.4 | Anodic Oxidation of Titanium in Phosphoric Acid (H ₃ PO ₄) | 2-49 |
| 2.8.5 | Anodic Oxidation of Titanium in Mixture of H ₂ SO ₄ , H ₂ O ₂ and H ₃ PO ₄ | 2-51 |
| 2.8.6 | Anodic Oxidation of Titanium in β-Glycerol Phosphate Disodium Salt Pentahydrate (β-GP) and Calcium Acetate Hydrate (CA) | 2-52 |

| | | |
|--|---|---------|
| 2.9 | Chemical Treatment | 2-54 |
| 2.9.1 | Acid Treatment | 2-54 |
| 2.9.2 | Gel Oxidation (Alkali and Heat Treatment) | 2-54 |
| CHAPTER 3: EXPERIMENTAL PROCEDURE | | 3-1 |
| 3.1 | Anodic Oxidation | 3-1 |
| 3.1.1 | Sample Preparation and Processing | 3-1 |
| 3.1.1.1 | Sulphuric Acid (H ₂ SO ₄) | 3-2 |
| 3.1.1.2 | Hydrogen Peroxide (H ₂ O ₂) | 3-2 |
| 3.1.1.3 | Phosphoric Acid (H ₃ PO ₄) | 3-2 |
| 3.1.1.4 | Mix Solution of H ₂ SO ₄ , H ₂ O ₂ and H ₃ PO ₄ | 3-3 |
| 3.1.1.5 | β-Glycerol Phosphate Disodium Salt Pentahydrate (β-GP) + Calcium Acetate Hydrate (CA) | 3-3 |
| 3.2 | Gel Oxidation | 3-4 |
| 3.2.1 | Sample Preparation | 3-4 |
| 3.2.1.1 | Soaking in NaOH (with stirrer) | 3-4 |
| 3.2.1.2 | Soaking in NaOH (without stirrer) | 3-5 |
| 3.3 | <i>In Vitro</i> | 3-6 |
| 3.3.1 | Simulated Body Fluid (SBF) Preparation | 3-6 |
| 3.3.2 | Soaking in SBF | 3-8 |
| 3.3.3 | Soaking in SBF under Ultraviolet (UV) Light | 3-9 |
| 3.3.4 | Culture Cell and Cell Morphology | 3-10 |
| 3.4 | Characterisation of Samples | 3-10 |
| 3.4.1 | Colour Measurement | 3-10 |
| 3.4.2 | Scanning Electron Microscopy (SEM) and Energy Dispersive Spectrometry (EDS) | 3-12 |
| 3.4.3 | Thickness (Colour Reflection) | 3-12 |
| 3.4.4 | Glancing Angle X-Ray Diffraction (GAXRD) | 3-13 |
| 3.4.5 | Laser Raman Microspectroscopy | 3-13 |
| 3.4.6 | Voltage and Current Measurement | 3-14 |

| | | |
|--|--|-------------|
| 3.4.7 | Scratch Testing | 3-14 |
| 3.4.8 | Cross-Section Imaging (Focussed Ion Beam Milling, FIB) | 3-17 |
| 3.4.9 | Atomic Force Microscopy (AFM) | 3-20 |
| CHAPTER 4: ANODIC OXIDATION OF TITANIUM | | 4-1 |
| 4.1 | ANODIC OXIDATION OF TITANIUM IN H₂SO₄ (Sample Series S) | 4-2 |
| 4.1.1 | Sample Preparation and Characterisation | 4-2 |
| 4.1.2 | Results and Discussion | 4-3 |
| 4.1.2.1 | Colour of Anodic Films | 4-3 |
| 4.1.2.2 | Microstructure (FESEM) | 4-12 |
| 4.1.2.3 | Mineralogy (Laser Raman Microspectroscopy) | 4-15 |
| 4.1.2.4 | Thicknesses | 4-20 |
| 4.1.2.5 | Applied Voltage and Current Density | 4-21 |
| 4.1.2.6 | <i>In Vitro</i> (Saos 2 Cultured cell) | 4-28 |
| 4.2 | ANODIC OXIDATION OF TITANIUM IN H₂O₂ (Sample Series H) | 4-33 |
| 4.2.1 | Sample Preparation and Characterisation | 4-33 |
| 4.2.2 | Results and Discussion | 4-33 |
| 4.2.2.1 | Colour of Anodic Films | 4-33 |
| 4.2.2.2 | Microstructure (FESEM) | 4-36 |
| 4.2.2.3 | Mineralogy (Laser Raman Microspectroscopy) and Thickness | 4-38 |
| 4.2.2.4 | Applied Voltage and Current Density | 4-43 |
| 4.2.2.6 | <i>In Vitro</i> (Saos 2 Cultured Cell) | 4-47 |
| 4.3 | ANODIC OXIDATION OF TITANIUM IN H₃PO₄ (Sample Series P) | 4-50 |
| 4.3.1 | Sample Preparation and Characterisation | 4-50 |
| 4.3.2 | Results and Discussion | 4-50 |
| 4.3.2.1 | Colour of Anodic Films | 4-50 |
| 4.3.2.2 | Microstructure (FESEM) | 4-53 |
| 4.3.2.3 | Mineralogy (Laser Raman Microspectroscopy) and Thickness | 4-56 |
| 4.3.2.4 | Applied Voltage and Current Density | 4-61 |
| 4.3.2.5 | <i>In Vitro</i> (Saos 2 Cultured Cell) | 4-63 |

| | |
|---|------|
| CHAPTER 5: ANODIC OXIDATION OF TITANIUM IN MIX SOLUTION | 5-1 |
| 5.1 Sample Preparation and Characterisation | 5-3 |
| 5.2 Results and Discussion | 5-4 |
| 5.2.1 Colour of Anodic Films | 5-4 |
| 5.2.2 Morphology of the Anodic Films (FESEM) | 5-6 |
| 5.2.3 Morphology of the Anodic Films (AFM) | 5-12 |
| 5.2.4 Mineralogy (Laser Raman Microspectroscopy) | 5-15 |
| 5.2.4.1 H ₂ SO ₄ (S) Core Electrolyte | 5-15 |
| 5.2.4.2 H ₂ SO ₄ + H ₂ O ₂ (SH) Mixture of Electrolytes | 5-16 |
| 5.2.4.3 H ₂ O ₂ + H ₃ PO ₄ (HP) Mixture of Electrolytes | 5-17 |
| 5.2.4.4 H ₂ SO ₄ + H ₃ PO ₄ (SP) Mixture of Electrolytes | 5-18 |
| 5.2.4.5 H ₂ SO ₄ + H ₃ PO ₄ + H ₂ O ₂ (SHP) Mixture of Electrolytes | 5-19 |
| 5.2.5 Mineralogy (Glancing-Angle X-Ray Diffraction, GAXRD) | 5-24 |
| 5.2.6 Thicknesses | 5-27 |
| 5.2.7 Applied Voltage and Current Density | 5-30 |
| 5.2.8 Morphology of the Cross-Section (FESEM, EDS & FIB) | 5-37 |
| 5.2.9 <i>In Vitro</i> Testing- Soaking in Simulated Body Fluid (SBF) | 5-41 |
| 5.2.10 Effect of Ultraviolet to Anodised Titanium in SBF | 5-46 |
| 5.2.11 <i>In Vitro</i> (Saos 2 Cultured Cell) | 5-50 |

| | |
|---|------|
| CHAPTER 6: ANODIC OXIDATION OF TITANIUM IN β-GP AND CA MIXTURE | 6-1 |
| 6.1 Sample Preparation and Characterisation | 6-2 |
| 6.2 Results and Discussion | 6-3 |
| 6.2.1 Colour of Anodic Films | 6-3 |
| 6.2.2 Mineralogy (Glancing Angle X-Ray Diffraction, GAXRD) | 6-5 |
| 6.2.3 Applied Voltage and Current Density | 6-25 |
| 6.2.4 Surface Morphology (Field Emission Scanning Electron Microscopy, FESEM) | 6-34 |
| 6.2.5 Cross-Section Focussed Ion Beam (FIB) Milling | 6-46 |
| 6.2.6 Effect of Ultraviolet Irradiation on Hydroxyapatite Formation on Anodised Titanium in SBF | 6-51 |
| 6.2.7 <i>In Vitro</i> (Saos 2 Cultured Cell) | 6-54 |

| | | |
|-------------------|---|-----|
| 8.1.3 | Anodic Oxidation in Organic Acid (β -Glycerophosphate + Calcium Acetate) | 8-4 |
| 8.2 | Gel Oxidation | 8-6 |
| REFERENCES | | R-1 |
| APPENDICES | | A-1 |

LIST OF FIGURES

| | | Page |
|--------------|--|------|
| Figure 2.1: | TiO ₂ photocatalysis general applications [11]. | 2-3 |
| Figure 2.2: | Phase diagram of the Ti-O system taken from Samsonov [20]. The region Ti ₂ O ₃ - TiO ₂ contains Ti ₂ O ₃ , Ti ₃ O ₅ , seven discrete phases of the homologous series Ti _n O _{2n-1} (Magneli phases) and TiO ₂ [8]. | 2-5 |
| Figure 2.3: | Crystal structure of anatase [8,12,22]. | 2-6 |
| Figure 2.4: | Crystal structure of rutile [12,22]. | 2-7 |
| Figure 2.5: | Crystal structure of brookite [11,22]. | 2-8 |
| Figure 2.6: | Ti-O phase diagram [25]. | 2-9 |
| Figure 2.7: | Proposed mechanism for the sintering and transformation of anatase into rutile. (adapted from [33]). | 2-13 |
| Figure 2.8: | Experimental data from previous researchers indicating that a linear correlation between TiO ₂ film density and refractive index is observed over for a wide range of values. Ottermann and Bange [39], Fitzgibbons et al. [40], Bendavid et al. [34], Hass [41], and Ribarsky [42] were used. (Adapted from [34]). | 2-14 |
| Figure 2.9: | Published values for the refractive index of single crystal anatase, taken from Meyer and Pietsch [44]; Hass [41]; Fitzgibbons [40]; Kingery et al. [46]; Washburn [47] and Kim [48]. The dispersive curve for single crystal rutile from Kim is also given [48]. | 2-16 |
| Figure 2.10: | Fundamental absorption edge of anatase and rutile single crystal, measured at a temperature of 10 K (adapted from [45]). | 2-17 |
| Figure 2.11: | The exponential dependence of the absorption coefficient of single crystal anatase, measured at 10 K with light polarised in E _⊥ c and E _∥ c directions (adapted from [45]). | 2-18 |
| Figure 2.12: | Major mechanism occurring on semiconductors: (a) electron–hole generation; (b) oxidation of donor (D); (c) reduction of acceptor (A); (d) and (e) electron–hole recombination at surface and in bulk, respectively [48]. | 2-19 |
| Figure 2.13: | Visible light (wavelength, 400-700nm) as part of electromagnetic energy [55]. | 2-21 |
| Figure 2.14: | RGB space colour cube (Red corner is hidden from view)[55]. | 2-21 |
| Figure 2.15: | HSV and HSL colour space [55]. | 2-22 |
| Figure 2.16: | CIE chromaticity diagram, (a) schematic and (b) Colour [55]. | 2-24 |
| Figure 2.17: | CIELAB chromaticity diagram [54]. | 2-25 |
| Figure 2.18: | Interference between two waves reflected at both surfaces of an oxidised titanium [61,63] | 2-26 |

| | | |
|--------------|---|------|
| Figure 2.19: | Schematic diagram of hard tissues in human body [17]. | 2-29 |
| Figure 2.20: | Bone screw and bone plate [17]. | 2-31 |
| Figure 2.21: | Bioactive titanium metal in a clinical hip joint system [4]. | 2-31 |
| Figure 2.22: | The screw-shaped artificial tooth [17]. | 2-31 |
| Figure 2.23: | (a) Brackets and buccal tubes (cpTi), (b) bracket, detail [18]. | 2-31 |
| Figure 2.24: | Schematic showing the relationship between the changes in surface structure and the potential of amorphous sodium titanate in the apatite formation process on its surface in an SBF [4]. | 2-35 |
| Figure 2.25: | Schematic of surface oxide film formation titanium and film reconstruction <i>in vivo</i> [197]. | 2-40 |
| Figure 2.26: | Schematic view of the oxide film on pure titanium [109]. | 2-42 |
| Figure 2.27: | Schematic diagram of the anodizing apparatus [112]. | 2-45 |
| | | |
| Figure 3.1: | Schematic diagram of anodic oxidation system [2]. | 3-1 |
| Figure 3.2: | Schematic of sample preparation in NaOH with stirrer. | 3-5 |
| Figure 3.3: | Schematic of sample preparation in NaOH without stirrer. | 3-6 |
| Figure 3.4: | Specimen surface area. | 3-9 |
| Figure 3.5: | Schematic of setup for UV irradiation of specimen during soaking in SBF. | 3-9 |
| Figure 3.6: | Interface of the software that was used to convert coordinate CIELAB to colour [8]. | 3-11 |
| Figure 3.7: | Schematic of thin film measurement using NanoCalc-2000 [9]. | 3-13 |
| Figure 3.8: | (a) Schematic of test method, (b) critical scratch load damage features in progressive load test [10]. | 3-15 |
| Figure 3.9: | Variation in measuring L_C using different methods. (a) Experimental results displayed on computer screen. (b) Scratch line captured by optical microscopy. (c) High-magnification view of scratch line where L_C was measured. | 3-17 |
| Figure 3.10: | Regular cross-section and clean-up milling. | 3-18 |
| Figure 3.11: | Sample tilted 45° (to normal) to observe cross section of the film. | 3-18 |
| Figure 3.12: | Schematic of the view for sample tilted 45° . | 3-19 |
| Figure 3.13: | Actual thickness for sample tilted 45° . | 3-19 |
| | | |
| Figure 4.1 : | Colours of film surfaces (1.5 M H_2SO_4 electrolyte) as a function of the applied voltage and the current density. | 4-4 |
| Figure 4.2: | Colours of film surfaces (1.5 M H_2SO_4 electrolyte) as a function of the applied voltage and the current density (conversion of CIELAB using computer software). | 4-5 |

| | | |
|--------------|---|------|
| Figure 4.3: | Brightness of samples oxidised at various current densities and different voltages in 1.5 M H ₂ SO ₄ electrolyte. | 4-8 |
| Figure 4.4: | Brightness of samples oxidised in H ₂ SO ₄ of varying concentrations for 5 mA.cm ⁻² current density. | 4-9 |
| Figure 4.5: | Brightness of samples oxidised in H ₂ SO ₄ of various concentrations for 10 mA.cm ⁻² current density. | 4-10 |
| Figure 4.6: | Thickness of samples oxidised in 1.5 M H ₂ SO ₄ at various current density for high voltage (100, 150, 250, and 350 V). | 4-11 |
| Figure 4.7: | Thickness of samples oxidised in 1.5 M H ₂ SO ₄ at various voltage for different current density (10, 20, 40, and 60 mA.cm ⁻²). | 4-11 |
| Figure 4.8: | FESEM images of film surfaces (1.5 M H ₂ SO ₄ electrolyte) as a function of applied voltage at 40 mA.cm ⁻² . | 4-14 |
| Figure 4.9: | Film thickness as a function of applied voltage, shown through laser Raman microspectroscopy patterns (A=anatase, main peak at 144 cm ⁻¹), interference colours, onset of detectable anatase formation, and effect of current density. | 4-16 |
| Figure 4.10: | Raman spectra of anodic films at 5 mA.cm ⁻² in solution of 1.5 M H ₂ SO ₄ for 100, 150, 200, 250, 300, and 350 V. | 4-18 |
| Figure 4.11: | Raman spectra of anodic films at 60 mA.cm ⁻² in solution of 1.5 M H ₂ SO ₄ for 100, 150, 200, 250, 300, and 350 V. | 4-19 |
| Figure 4.12: | Graph of current density as a function of time for titanium anodising in H ₂ SO ₄ of different concentrations at 5 mA.cm ⁻² and 350 V. | 4-22 |
| Figure 4.13: | Graph of current density as a function of time for titanium anodising in H ₂ SO ₄ of different concentrations at 60 mA.cm ⁻² and 350 V. | 4-22 |
| Figure 4.14: | Graph of voltage as a function of time for titanium anodising in H ₂ SO ₄ of different concentrations at 5 mA.cm ⁻² and 350 V. | 4-24 |
| Figure 4.15: | Graph of voltage as a function of time for titanium anodising in H ₂ SO ₄ of different concentrations at 60 mA.cm ⁻² for 350 V. | 4-24 |
| Figure 4.16: | Diagram of anodisation process. | 4-26 |
| Figure 4.17: | FESEM images of cell attachment on Ti under different surface modification conditions at low (a, b, c, and d) and high (e, f, g, and h) magnifications: (a) Ti, (b) anodised Ti in 1.5 M H ₂ SO ₄ (5 mA.cm ⁻² , 180 V, 50 min), (c) anodised Ti in 1.5 M H ₂ SO ₄ (60 mA.cm ⁻² , 350 V, 10 min) and (d) anodised Ti in 1.5 M H ₂ SO ₄ (60 mA.cm ⁻² , 250 V, 10 min). | 4-30 |
| Figure 4.18: | Colours of film surfaces (0.3 M H ₂ O ₂ electrolyte) as a function of the applied voltage and current density | 4-34 |
| Figure 4.19: | Colours of film surfaces (0.3 M H ₂ O ₂ electrolyte) as a function of the applied voltage and current density (conversion of CIELAB using computer software). | 4-34 |

| | | |
|--------------|--|------|
| Figure 4.20: | Brightness of samples oxidised at various current densities and different voltages in 0.3 M H ₂ O ₂ electrolyte. | 4-35 |
| Figure 4.21: | FESEM images of film surfaces (0.3 M H ₂ O ₂ electrolyte) as a function of applied voltage at 40 mA.cm ⁻² . | 4-37 |
| Figure 4.22: | Film thickness as a function of applied voltage, shown through laser Raman microspectroscopy patterns (A=anatase, main peak at 144 cm ⁻¹), interference colours, onset of detectable anatase formation, and effect of current density. | 4-40 |
| Figure 4.23: | Raman spectra of anodic films at 5 mAcm ⁻² in solution of 0.3 M H ₂ O ₂ for 100, 150, 200, 250, 300, and 350 V. | 4-41 |
| Figure 4.24: | Raman spectra of anodic films at 60 mA.cm ⁻² in solution of 0.3 M H ₂ O ₂ for 100, 150, 200, 250, 300, and 350 V. | 4-42 |
| Figure 4.25: | Graph of voltage vs. time and current density vs. time for titanium anodic oxidation in 0.3 M H ₂ O ₂ electrolyte at 5 mA.cm ⁻² for 350 V. | 4-43 |
| Figure 4.26: | Growth of the anodised film in H ₂ O ₂ electrolyte. | 4-44 |
| Figure 4.27: | Graph of voltage vs. time and current density vs. time for titanium anodic oxidation in 0.3 M H ₂ O ₂ electrolyte at 60 mA.cm ⁻² for 350 V. | 4-45 |
| Figure 4.28: | Electrical behaviour of the anodic oxidation in H ₂ O ₂ electrolyte at low current density. | 4-46 |
| Figure 4.29: | Electrical behaviour of the anodic oxidation in H ₂ O ₂ electrolyte at high current density. | 4-47 |
| Figure 4.30: | FESEM images of cell attachment on Ti surface at (a) low (c) high magnifications and on Ti (anodised) in 0.3 M H ₂ O ₂ (40 mA, 350V, and 10 min) at (b) low (d) high magnifications. | 4-48 |
| Figure 4.31: | Colours of film surfaces (0.3 M H ₃ PO ₄ electrolyte) as a function of applied voltages and current densities. | 4-51 |
| Figure 4.32: | Colours of film surfaces (0.3 M H ₃ PO ₄ electrolyte) as a function of applied voltages and current densities (conversion of CIELAB using computer software). | 4-51 |
| Figure 4.33: | Brightness of samples oxidised at various current densities and voltages in 0.3 M H ₃ PO ₄ electrolyte. | 4-52 |
| Figure 4.34: | FESEM images of the film surfaces (0.3 M H ₃ PO ₄ electrolyte) as a function of the applied voltage at 40 mA.cm ⁻² . | 4-54 |
| Figure 4.35: | Film thickness as a function of applied voltage, shown through laser Raman microspectroscopy patterns (A=anatase, main peak at 144 cm ⁻¹), interference colours, onset of detectable anatase formation, and effect of current density. | 4-57 |
| Figure 4.36: | Raman spectra of anodic films at 5 mA.cm ⁻² in solution of 0.3 M H ₃ PO ₄ for 100, 150, 200, 250, 300, and 350 V. | 4-59 |

| | | |
|-----------------|---|------|
| Figure 4.37: | Raman spectra of anodic films at 60 mA.cm ⁻² in solution of 0.3 M H ₃ PO ₄ for 100, 150, 200, 250, 300, and 350 V. | 4-60 |
| Figure 4.38: | Graph of voltage vs. time and current density vs. time for titanium anodic oxidation in 0.3 M H ₃ PO ₄ electrolyte at 5 mA.cm ⁻² for 350 V. | 4-61 |
| Figure 4.39: | Graph of voltage vs. time and current density vs. time for titanium anodic oxidation in 0.3 M H ₃ PO ₄ electrolyte at 60 mA.cm ⁻² for 350 V. | 4-63 |
| Figure 4.40: | FESEM images of cell attachment on Ti surface at (a) low (c) high magnifications and on Ti (anodised) in 0.3 M H ₃ PO ₄ (40 mA.cm ⁻² , 350V, 10 min) at (b) low (d) high magnifications. | 4-64 |
| | | |
| Figure 5.1: | Variation of the colour of the film surface for S at different voltages (90 to 180 V) and different anodisation times (1, 3, 5, 10, 30 and 50 min) at 5 mA.cm ⁻² . | 5-5 |
| Figure 5.2: | Variation of the colour of the film surface for SH at different voltages (90 to 180 V) and different anodisation times (1, 3, 5, 10, 30 and 50 min) at 5 mA.cm ⁻² . | 5-5 |
| Figure 5.3: | Variation of the colour of the film surface for HP at different voltages (90 to 180 V) and different anodisation times (1, 3, 5, 10, 30 and 50 min) at 5 mA.cm ⁻² . | 5-5 |
| Figure 5.4: | Variation of the colour of the film surface for SP at different voltages (90 to 180 V) and different anodisation times (1, 3, 5, 10, 30 and 50 min) at 5 mA.cm ⁻² . | 5-5 |
| Figure 5.5: | Variation of the colour of the film surface for SHP at different voltages (90 to 180 V) and different anodisation times (1, 3, 5, 10, 30 and 50 min) at 5 mA.cm ⁻² . | 5-6 |
| Figure 5.6: | FESEM images for sample S, SH, HP, SP and SHP at 90 V and 180 V for 1 min anodisation. | 5-7 |
| Figure 5.7: | FESEM images for sample S, SH, HP, SP and SHP at 90 V and 180 V for 50 min anodisation. | 5-8 |
| Figure 5.8: | FESEM images for sample SHP at 90, 120, 150, and 180 V for 1 and 50 min anodisation. | 5-9 |
| Figure 5.9: | FESEM images for sample SHP at 90 V for 1, 3, 5, 10, 30, and 50 min anodisation. | 5-11 |
| Figure 5.10: | FESEM images for sample SHP at 180 V for 1, 3, 5, 10, 30, and 50 min anodisation. | 5-12 |
| Figure 5.11(a): | AFM images of anodic titanium oxide film on Ti surface in solution SHP at 90 V for 1 min. | 5-13 |
| Figure 5.11(b): | AFM images of anodic titanium oxide film on Ti surface in solution SHP at 90 V for 50 min. | 5-14 |

| | |
|--|------|
| Figure 5.12(a): AFM images of anodic titanium oxide film on Ti surface in solution SHP at 180 V for 1 min. | 5-14 |
| Figure 5.12(b): AFM images of anodic titanium oxide film on Ti surface in solution SHP at 180 V for 50 min. | 5-15 |
| Figure 5.13: Raman intensity of anatase main peak (144 cm^{-1}) vs. anodisation time of anodic films formed at 90 and 180 V in solution S. | 5-16 |
| Figure 5.14: Raman intensity of anatase main peak (144 cm^{-1}) vs. anodisation time of anodic films formed at 90 and 180 V in solution SH. | 5-17 |
| Figure 5.15: Raman intensity of anatase main peak (144 cm^{-1}) vs. anodisation time of anodic films formed at 90 and 180 V in solution HP. | 5-18 |
| Figure 5.16: Raman intensity anatase main peak (144 cm^{-1}) vs. anodisation time of anodic films formed at 90 and 180 V in solution SP. | 5-19 |
| Figure 5.17: Raman intensity of anatase main peak (144 cm^{-1}) vs. anodisation time of anodic films formed at 90 and 180 V in solution SHP. | 5-20 |
| Figure 5.18: Raman intensity of anatase main peak (144 cm^{-1}) vs. voltage of anodic films formed at 90, 120, 150 and 180 V in solution SHP. | 5-21 |
| Figure 5.19: Raman intensity of anatase main peak of anodic films formed at 90 and 180 V for 1 min in solution S, SH, HP, SP, and SHP. | 5-22 |
| Figure 5.20: Raman intensity of anatase main peak of anodic films formed at 90 and 180 V for 50 min in solution S, SH, HP, SP, and SHP. | 5-23 |
| Figure 5.21: Glancing angle XRD patterns of anodic films at 180 V in SHP solution for: 1, 3, 5, 10, 30, and 50 min. | 5-26 |
| Figure 5.22: Variation of anodic film thickness as a function of time at 180V in solutions S, SH, HP, SP and SHP. | 5-28 |
| Figure 5.23: Variation of anodic film thickness as a function of time in solution SHP at 90 V, 120 V, 150 V, and 180 V. | 5-29 |
| Figure 5.24: Sequence of oxide formation. (1) Metal reacts with electrolyte. (2) Passive gel is formed on the metal surface. (3) Metal oxide is formed on the gel after anodising. | 5-29 |
| Figure 5.25: Variation of current density as a function of anodisation time in SHP at 90, 120, 150, and 180 V. | 5-30 |
| Figure 5.26: Variation of applied voltages as a function of anodisation time in SHP at 90, 120, 150, and 180 V. | 5-31 |
| Figure 5.27: Electrical behaviour of the anodic oxidation in SHP electrolyte. | 5-32 |

| | | |
|--------------|--|------|
| Figure 5.28: | Current density behaviour of the anodic oxidation in SHP electrolyte. | 5-33 |
| Figure 5.29: | Variation of current density as a function of anodisation times at 90V for S, SH, HP, SP, and SHP. | 5-35 |
| Figure 5.30: | Variation of applied voltages as a function of anodisation times at 90 V for S, SH, HP, SP, and SHP. | 5-35 |
| Figure 5.31: | Variation of current density as a function of anodisation times at 180 V for S, SH, HP, SP, and SHP. | 5-36 |
| Figure 5.32: | Variation of applied voltages as a function of anodisation times at 180 V for S, SH, HP, SP, and SHP. | 5-36 |
| Figure 5.33: | (a) FESEM image of the Ti/TiO _{2-x} interface for sample SHP at 180 V for 50 min and (b) EDS data for the region. | 5-39 |
| Figure 5.34: | Cross section of the films S, SH, HP, SP, and SHP anodised at 180 V for 50 min (white bar indicated oxide layer thickness; tilted 45° to normal). | 5-40 |
| Figure 5.35: | FESEM images of SHP sample at different applied voltages (90,120, 150 and 180 V) for 50 min, before and after 7 days soaking in SBF (arrows indicate hydroxyapatite). | 5-41 |
| Figure 5.36: | EDS of SHP sample at 90 V for 50 min after 7 days soaking in SBF. | 5-42 |
| Figure 5.37: | EDS of SHP sample at 180 V for 50 min after 7 days soaking in SBF. | 5-43 |
| Figure 5.38: | FESEM images (low- and high-magnification of insets) of samples anodised in SHP at 180 V for different anodisation times (1, 3, 5, 10, 30 and 50 min) after 7 days soaking in SBF. | 5-44 |
| Figure 5.39: | EDS of SHP sample at 180 V for 1 min after 7 days soaking in SBF. | 5-45 |
| Figure 5.40: | Cross-section of the sample anodised in SHP at 180 V for 50 min, before and after 7 days soaking in SBF (tilted at 45°). | 5-46 |
| Figure 5.41: | FESEM images of the samples anodised in different electrolytes (S, SH, HP, SP and SHP) at 180 V for 50 min after soaking in SBF for 3 days. | 5-47 |
| Figure 5.42: | FESEM images of the samples anodised in different electrolytes (S, SH, HP, SP and SHP) at 180 V for 50 min after soaking in SBF under UV irradiation for 3 days. | 5-48 |
| Figure 5.43: | EDS of SHP sample at 180 V (50 min) after 3 days soaking in SBF (under UV irradiation). | 5-49 |
| Figure 5.44: | FESEM images of cell attachment on the anodised Ti in SHP (5 mA.cm ⁻² , 180 V, 50 min) at low (a,b) and high (c,d) magnification. | 5-51 |

| | | |
|--------------|--|------|
| Figure 6.1: | Colours of film surfaces (0.02 M β -GP + 0.2 M CA, 10 mA.cm ⁻²) as a function of the applied voltage and anodisation time. | 6-4 |
| Figure 6.2: | Colours of film surfaces (0.02 M β -GP + 0.2 M CA, 20 mA.cm ⁻²) as a function of the applied voltage and anodisation time. | 6-4 |
| Figure 6.3: | Colours of film surfaces (0.04 M β -GP + 0.4 M CA, 10 mA.cm ⁻²) as a function of the applied voltage and anodisation time. | 6-5 |
| Figure 6.4: | Colours of film surfaces (0.04 M β -GP + 0.4 M CA, 20 mA.cm ⁻²) as a function of the applied voltage and anodisation time. | 6-5 |
| Figure 6.5: | GAXRD patterns of the samples anodised in 0.02 M β -GP + 0.2 M CA, current density 10 mA.cm ⁻² at 150 V for 1, 3, 5, and 10 min. | 6-7 |
| Figure 6.6: | GAXRD patterns of the samples anodised in 0.02 M β -GP + 0.2 M CA, current density 10 mA.cm ⁻² at 350 V for 1, 3, 5, and 10 min. | 6-8 |
| Figure 6.7: | GAXRD patterns of the samples anodised in 0.02 M β -GP + 0.2 M CA, current density 10 mA.cm ⁻² at 150, 200, 250, 300, and 350 V for 10 min. | 6-9 |
| Figure 6.8: | GAXRD patterns of the samples anodised in 0.02 M β -GP + 0.2 M CA, current density 20 mA.cm ⁻² at 150 V for 1, 3, 5, and 10 min. | 6-11 |
| Figure 6.9: | GAXRD patterns of the samples anodised in 0.02 M β -GP + 0.2 M CA, current density 20 mA.cm ⁻² at 350 V for 1, 3, 5, and 10 min. | 6-12 |
| Figure 6.10: | GAXRD patterns of the samples anodised in 0.02 M β -GP + 0.2 M CA, current density 20 mA.cm ⁻² at 150, 200, 250, 300, and 350 V for 10 min. | 6-13 |
| Figure 6.11: | GAXRD patterns of the samples anodised in 0.04 M β -GP + 0.4 M CA, current density 10 mA.cm ⁻² at 150 V for 1, 3, 5, and 10 min. | 6-15 |
| Figure 6.12: | GAXRD patterns of the samples anodised in 0.04 M β -GP + 0.4 M CA, current density 10 mA.cm ⁻² at 350 V for 1, 3, 5, and 10 min. | 6-16 |
| Figure 6.13: | GAXRD patterns of the samples anodised in 0.04 M β -GP + 0.4 M CA, current density 10 mA.cm ⁻² at 150, 200, 250, 300, and 350 V for 10 min. | 6-17 |
| Figure 6.14: | GAXRD patterns of the samples anodised in 0.04 M β -GP + 0.4 M CA, current density 20 mA.cm ⁻² at 150 V for 1, 3, 5, and 10 min. | 6-20 |

| | | |
|--------------|---|------|
| Figure 6.15: | GAXRD patterns of the samples anodised in 0.04 M β -GP + 0.4 M CA, current density 20 mA.cm ⁻² at 350 V for 1, 3, 5, and 10 min. | 6-21 |
| Figure 6.16: | GAXRD patterns of the samples anodised in 0.04 M β -GP + 0.4 M CA, current density 20 mA.cm ⁻² at 150, 200, 250, 300, and 350 V for 10 min. | 6-22 |
| Figure 6.17: | Schematic diagram illustrating the formation of crystalline oxide in an anodic film on titanium. | 6-24 |
| Figure 6.18: | Graph of voltage vs. time and current density vs. time for titanium anodic oxidation in 0.02 M β -GP + 0.2 M CA electrolyte at 10 mA.cm ⁻² for 150 V. | 6-26 |
| Figure 6.19: | Graph of voltage vs. time and current density vs. time for titanium anodic oxidation in 0.04 M β -GP + 0.4 M CA electrolyte at 10 mA.cm ⁻² for 150 V. | 6-26 |
| Figure 6.20: | Conceptual model models incorporate applied voltage, current density, and anodisation time. | 6-27 |
| Figure 6.21: | Model for current density as a function of time. | 6-27 |
| Figure 6.22: | Model for voltage as a function of time. | 6-28 |
| Figure 6.23: | Graph for voltage vs. time and current density vs. time for titanium anodic oxidation in 0.02 M β -GP + 0.2 M CA electrolyte at 10 mA.cm ⁻² for 350 V | 6-33 |
| Figure 6.24: | Graph for voltage vs. time and current density vs. time for titanium anodic oxidation in 0.04 M β -GP + 0.4 M CA electrolyte at 10 mA.cm ⁻² for 350 V. | 6-34 |
| Figure 6.25: | FESEM micrographs of anodised surfaces in 0.02 M β -GP + 0.2 M CA (10 mA.cm ⁻²) at 150 V and 350 V for 1, 3, 5 and 10 min. | 6-38 |
| Figure 6.26: | FESEM micrographs of anodised surfaces in 0.02 M β -GP + 0.2 M CA(10 mA.cm ⁻²) at 150 V, 200 V, 250 V, 300 V, and 350 V for 10 min. | 6-39 |
| Figure 6.27: | FESEM micrographs of anodised surfaces in 0.02 M β -GP + 0.2 M CA (20 mA.cm ⁻²) at 150 V and 350 V for 1, 3, 5 and 10 min. | 6-40 |
| Figure 6.28: | FESEM micrographs of anodised surfaces in 0.02 M β -GP + 0.2 M CA (20 mA.cm ⁻²) at 150 V, 200 V, 250 V, 300 V, and 350 V for 10 min. | 6-41 |
| Figure 6.29: | FESEM micrographs of anodised surfaces in 0.04 M β -GP + 0.4 M CA (10 mA.cm ⁻²) at 150 V and 350 V for 1, 3, 5 and 10 min | 6-42 |
| Figure 6.30: | FESEM micrographs of anodised surfaces in 0.04 M β -GP + 0.4 M CA (10 mA.cm ⁻²) at 150 V, 200 V, 250 V, 300 V, and 350 V for 10 min | 6-43 |

| | | |
|----------------|--|------|
| Figure 6.31: | FESEM micrographs of anodised surfaces in 0.04 M β -GP + 0.4 M CA (20 mA.cm ⁻²) at 150 V and 350 V for 1, 3, 5 and 10 min. | 6-44 |
| Figure 6.32: | FESEM micrographs of anodised surfaces in 0.04 M β -GP + 0.4 M CA (20 mA.cm ⁻²) at 150 V, 200 V, 250 V, 300 V, and 350 V for 10 min | 6-45 |
| Figure 6.33: | FIB micrographs of the cross sections for samples 0.02 M β -GP + 0.2 M CA and 0.04 M β -GP + 0.4 M CA at 10 and 20 mA.cm ⁻² for 10 min | 6-48 |
| Figure 6.34: | FESEM images of the samples anodised in 0.02 M β -GP + 0.2 M CA, current densities 10 and 20 mA.cm ⁻² at 150 and 350 V for 10 min after soaking in SBF for 7 days. | 6-50 |
| Figure 6.35: | FESEM images of the samples anodised in 0.04 M β -GP + 0.4 M CA, current densities 10 and 20 mA.cm ⁻² at 150 and 350 V for 10 min after soaking in SBF for 7 days. | 6-50 |
| Figure 6.36: | EDS pattern of the samples anodised in 0.02 M β -GP + 0.2 M CA, current densities 10 mA.cm ⁻² at 150 V for 10 min after soaking in SBF for 7 days. | 6-51 |
| Figure 6.37: | FESEM images of the samples anodised in 0.02 M β -GP + 0.2 M CA, current densities 10 and 20 mA.cm ⁻² at 150 and 350 V for 10 min after soaking in SBF for 3 days under UV light. | 6-52 |
| Figure 6.38: | FESEM images of the samples anodised in 0.04 M β -GP + 0.4 M CA, current densities 10 and 20 mA.cm ⁻² at 150 and 350 V for 10 min after soaking in SBF for 3 days under UV light. | 6-52 |
| Figure 6.39: | EDS pattern of the samples anodised in 0.02 M β -GP + 0.2 M CA, current densities 10 mA.cm ⁻² at 150 V for 10 min after soaking in SBF (under UV irradiation) for 3 days. | 6-53 |
| Figure 6.40: | EDS pattern of the samples anodised in 0.04 M β -GP + 0.4 M CA, current densities 10 mA.cm ⁻² at 350 V for 10 min after soaking in SBF (under UV irradiation) for 3 days. | 6-54 |
| Figure 6.41: | FESEM images showing cell attachment on the anodised Ti in 0.04 M β -GP + 0.4 M CA (10 mA.cm ⁻² , 350V, 10 min) at low (a,b) and high (c,d) magnifications. | 6-55 |
| Figure 7.1(a): | Schematic of gelation and oxidation processes for low concentration (0.5 M NaOH and 1.0 M NaOH; a = amorphous; c = crystalline). | 7-5 |
| Figure 7.1(b): | Schematic of gelation and oxidation processes for high concentration, 5.0 M NaOH; a = amorphous; c = crystalline). | 7-6 |
| Figure 7.1(c): | Schematic of gelation and oxidation processes for high concentration, 10.0 M NaOH; a = amorphous; c = crystalline). | 7-6 |
| Figure 7.2: | Colour of titanium surface after NaOH treatment at different concentrations and oxidation temperatures. | 7-7 |

| | | |
|--------------|---|------|
| Figure 7.3: | GAXRD patterns of the surfaces of Ti treated in 0.5 M NaOH after being subjected to oxidation at various temperatures | 7-10 |
| Figure 7.4: | GAXRD patterns of the surfaces of Ti treated in 1.0 M NaOH after being subjected to oxidation at various temperatures. | 7-11 |
| Figure 7.5: | GAXRD patterns of the surfaces of Ti treated in 5.0 M NaOH after being subjected to oxidation at various temperatures. | 7-12 |
| Figure 7.6: | GAXRD patterns of the surfaces of Ti treated in 10.0 M NaOH after being subjected to oxidation at various temperatures. | 7-13 |
| Figure 7.7: | FESEM images of the surface of Ti heated with NaOH (0.5 and 1.0 M) and subjected to oxidations at various temperatures. (Low Magnification, 6000 X). | 7-15 |
| Figure 7.8: | FESEM images of the surface of Ti treated with NaOH (5.0 and 10.0 M) and subjected to oxidations at various temperatures. (Low Magnification, 6000 X). | 7-16 |
| Figure 7.9: | FESEM images of the surface of Ti treated with NaOH (0.5 and 1.0 M) and subjected to oxidations at various temperatures. (High magnification, 30000 X). | 7-17 |
| Figure 7.10: | FESEM images of the surface of Ti treated with NaOH (5.0 and 10.0 M) and subjected to oxidations at various temperatures. (High magnification, 30000 X). | 7-18 |
| Figure 7.11: | Cross-sectional images of the Ti treated with NaOH (0.5 and 1.0 M) followed by oxidations at various temperatures (white bar indicates oxide layer thickness; tilted 45° to normal). | 7-22 |
| Figure 7.12: | Cross-sectional images of the Ti treated with NaOH (5.0 and 10.0 M) followed by oxidations at various temperatures (white bar indicates oxide layer thickness; tilted 45° to normal). | 7-23 |
| Figure 7.13: | Thickness of films treated in NaOH (0.5, 1.0, 5.0, and 10.0 M) at various oxidation temperature (400°, 600°, and 800°C). | 7-24 |
| Figure 7.14: | FESEM images of the surface of the Ti surface treated with NaOH (5.0 M and 5.0 M, 400°C) after soaking in SBF for 1 and 3 days. | 7-26 |
| Figure 7.15: | FESEM images of the surface of the Ti treated with NaOH (5.0 M, 600°C and 5.0 M, 800°C) after soaking in SBF for 1 and 3 days. | 7-27 |
| Figure 7.16: | FESEM images of the surface of the Ti treated with NaOH (10.0 and 10.0 M, 400°C) after soaking in SBF for 1 and 3 days. | 7-28 |
| Figure 7.17: | FESEM images of the surface of the Ti treated with NaOH (10.0 M, 600°C and 10.0 M, 800°C) after soaking in SBF for 1 and 3 days. | 7-29 |
| Figure 7.18: | GAXRD patterns of the surfaces of the Ti treated with 5.0 M NaOH after being subjected to oxidation at various temperatures after soaking for 1 day in SBF. | 7-32 |

| | | |
|--------------|---|------|
| Figure 7.19: | GAXRD patterns of the surfaces of the Ti surface treated with 10.0 M NaOH and then subjected to oxidation at various temperatures after soaking for 1 day in SBF. | 7-33 |
| Figure 7.20: | FESEM images of the surfaces of Ti substrates treated with 5 M NaOH and oxidised at 400°, 600°, and 800°C for 1 h, followed by soaking in SBF irradiation with UV light for 1 day. | 7-34 |
| Figure 7.21: | GAXRD patterns of the surfaces of the Ti treated with 5.0 M NaOH which was subjected to oxidation at various temperatures and soaked in SBF under UV irradiation (15 min on and off alternately) for 1 day. | 7-35 |
| Figure 7.22: | FESEM images of cell attachment on Ti surface at low (a,b) and high (c,d) magnifications for (a) Ti and (b) Ti treated with 5.0 M NaOH (60°C, 24 h) followed by oxidation at 400°C. | 7-39 |
| Figure 7.23: | GAXRD patterns of the surfaces of the 0.5 M NaOH-treated Ti (stirrer) subject to oxidations at various temperatures. | 7-44 |
| Figure 7.24: | GAXRD patterns of the surfaces of the 1.0 M NaOH-treated Ti (stirrer) subject to oxidations at various temperatures. | 7-45 |
| Figure 7.25: | GAXRD patterns of the surfaces of the 5.0 M NaOH-treated Ti (stirrer) subject to oxidations at various temperatures. | 7-46 |
| Figure 7.26: | GAXRD patterns of the surfaces of the 10.0 M NaOH-treated Ti (stirrer) subject to oxidations at various temperatures. | 7-47 |
| Figure 7.27: | Boundary layer concept in corrosion [178]. | 7-48 |
| Figure 7.28: | Raman spectra of the surfaces of samples prepared using 0.5 M NaOH at different temperatures. | 7-49 |
| Figure 7.29: | Raman spectra of the surfaces of samples prepared using 1.0 M NaOH at different temperatures. | 7-50 |
| Figure 7.30: | Raman V of the surfaces of samples prepared using 5.0 M NaOH at different temperatures. | 7-50 |
| Figure 7.31: | Raman spectra of the surfaces of samples prepared using 10.0 M NaOH at different temperatures. | 7-51 |
| Figure 7.32: | Thicknesses of all titanium substrates as a function of NaOH concentration and oxidation temperatures. | 7-52 |
| Figure 7.33: | FESEM images of the surface of NaOH (0.5 and 1.0 M) treated Ti subjected to oxidations at various temperatures (Magnification, 6000 X). | 7-54 |
| Figure 7.34: | FESEM images of the surface of NaOH (5.0 and 10.0 M) treated Ti subjected to oxidations at various temperatures. (Magnification, 6000 X). | 7-55 |

LIST OF TABLES

| | Page |
|--|------|
| Table 1.1: Type of implant - tissue response [1]. | 1-1 |
| Table 2.1: The applications of TiO ₂ in various fields. | 2-2 |
| Table 2.2: The applications of photocatalysis [7]. | 2-3 |
| Table 2.3: Applications of TiO ₂ in biomedical fields. | 2-4 |
| Table 2.4: Properties of titanium oxides at various oxidation states [12,23]. | 2-6 |
| Table 2.5: The special points of the Ti-O phase diagram [25]. | 2-10 |
| Table 2.6: Ti-O crystal structure data [25]. | 2-11 |
| Table 2.7: Bulk properties of the three main polymorphs TiO ₂ (anatase, brookite and rutile) [8]. | 2-12 |
| Table 2.8: Various density of TiO ₂ [9]. | 2-13 |
| Table 2.9: Hue value and colours. | 2-22 |
| Table 2.10: The HSV (saturation and value) and HSL (saturation and lightness) [58]. | 2-23 |
| Table 2.11: The value of the coordinate CIELAB. | 2-25 |
| Table 2.12: Some basic properties of titanium [17]. | 2-27 |
| Table 2.13: Mechanical properties of titanium and it alloys [17]. | 2-28 |
| Table 2.14: The applications of Titanium and its alloys in biomedical field. | 2-30 |
| Table 2.15: Other applications of Titanium and its alloys. | 2-33 |
| Table 2.16: Chemical composition of the simulated body fluids and blood plasma (mM)[4]. | 2-34 |
| Table 2.17: Schematic presentation of different stages in adhesion and spreading cell in vitro [87]. | 2-37 |
| Table 2.18: Attached cell were divided into three types of spreading [83, 87] | 2-38 |
| Table 2.19: Surface properties that affect the human osteoblast-like cell behaviour. | 2-39 |
| Table 2.20: Method of TiO ₂ fabrication for single crystal and polycrystalline, thin and thick films. | 2-41 |
| Table 2.21: Surface modification methods for titanium [17]. | 2-44 |
| Table 2.22: Parameters and results from studies on biomaterials applications using H ₂ SO ₄ as an electrolyte. | 2-48 |
| Table 2.23: Summary of studies on hydrogen peroxide (H ₂ O ₂) treatment. | 2-49 |
| Table 2.24: Summary of studies on biomaterials applications using H ₃ PO ₄ as an electrolyte. | 2-51 |

| | |
|---|------|
| Table 2.25: The effect of applied voltage and electrolyte to chemical composition of oxide. | 2-53 |
| Table 2.26: Summary of alkali treatments used for surface modification of titanium. | 2-55 |
| Table 3.1: Parameters used for anodic oxidation in H ₂ SO ₄ . | 3-2 |
| Table 3.2: Parameters used for anodic oxidation in H ₂ O ₂ . | 3-2 |
| Table 3.3: Parameters used for anodic oxidation in H ₃ PO ₄ . | 3-3 |
| Table 3.4: Parameters used for anodic oxidation in mixed solution. | 3-3 |
| Table 3.5: Parameters used for anodic oxidation in β-GP + CA. | 3-4 |
| Table 3.6: Gelation treatment conditions for samples. | 3-5 |
| Table 3.7: Gelation treatment conditions for all samples (without stirring in NaOH). | 3-6 |
| Table 3.8: The order, amounts, weighing containers, purities and formula weights of reagents used for preparing 1000 mL of SBF by Kokubo <i>et al.</i> [5]. | 3-7 |
| Table 3.9: Comparison of nominal ion concentration of SBF to human blood plasma [5]. | 3-7 |
| Table 3.10: The order, amounts, purities, formula weights and supplier of reagents used for preparing 1000 mL of SBF used in this study. | 3-8 |
| Table 3.11: The value of the coordinate CIELAB [7]. | 3-11 |
| Table 3.12: Scratch test parameters. | 3-15 |
| Table 4.1: Parameters used for anodic oxidation in H ₂ SO ₄ . | 4-2 |
| Table 4.2: Effect of voltage on the microstructure. | 4-12 |
| Table 4.3: Three types of anodised samples. | 4-15 |
| Table 4.4: Comparison between different studies on anodic oxidation. | 4-20 |
| Table 4.5: Shape of anodisation curve from others studies. | 4-26 |
| Table 4.6: Discharge and maximum voltages attained at 60 mA.cm ⁻² for 10 min. | 4-27 |
| Table 4.7: Observations from FESEM images and mineralogy of the samples shown in Figure 4.17. | 4-31 |
| Table 4.8: Parameters in anodic oxidation experiments in H ₂ O ₂ . | 4-33 |
| Table 4.9: Effect of voltage on microstructure. | 4-38 |
| Table 4.10: Summary of observations from FESEM images and mineralogy of the samples shown by Figure 4.27. | 4-48 |
| Table 4.11: Parameters used for anodic oxidation in H ₃ PO ₄ . | 4-50 |
| Table 4.12: Effect of voltage on microstructure. | 4-53 |

| | |
|--|------|
| Table 4.13: Properties of electrolyte. | 4-55 |
| Table 4.14: Summary of observations from FESEM images and mineralogy of the samples shown by Figure 4.37. | 4-64 |
| Table 5.1: Parameters Used for Anodic Oxidation. | 5-3 |
| Table 5.2: Colour changes with different parameters. | 5-4 |
| Table 5.3: Description of samples SHP after 1 and 50 min of anodisation at 90 V and 180 V. | 5-12 |
| Table 5.4: Raman spectra for rutile and anatase [159]. | 5-15 |
| Table 5.5: The pore size and thickness of anodic films formed in various. | 5-24 |
| Table 5.6: Comparison between studies on anodic oxidation of Ti. | 5-25 |
| Table 5.7: EDS chemical analyses based on data in Figure 5.31(b). | 5-37 |
| Table 5.8: Summary of observations from FESEM images and mineralogy of the samples (Figure 5.42). | 5-51 |
| Table 5.9: Observation and properties of Ti and TiO ₂ that affect the cell attachment. | 5-52 |
| Table 6.1: Parameters used for anodic oxidation in β -GP + CA. | 6-2 |
| Table 6.2: Parameters for studies depicted in Figure 6.5, 6.6 and 6.7. | 6-6 |
| Table 6.3: Parameters for the studies depicted in Figure 6.8 - 6.10. | 6-10 |
| Table 6.4: Parameters for studies depicted in Figure 6.11- 6.13. | 6-14 |
| Table 6.5: Parameters used in studies shown in Figure 6.14, 6.15 and 6.16. | 6-18 |
| Table 6.6: The effect of the concentration of the electrolyte and the current density on the mineral phases formed in the oxide layer. | 6-23 |
| Table 6.7: Summary of anodic oxidation in 0.02 M β -GP + 0.2 M CA and 0.04 M β -GP + 0.4 M CA at 150 V. | 6-23 |
| Table 6.8: Summary of anodic oxidation results in 0.02 M β -GP + 0.2 M CA and 0.04 M β -GP + 0.4 M CA at 350 V. | 6-25 |
| Table 6.9: Summary of conditions of the samples seen in Figure 6.26 - 6.33. | 6-32 |
| Table 6.10: The effect of the voltage, time, current density and electrolyte concentration on the microstructure. | 6-34 |
| Table 6.11: Summary of observations from FESEM images and the mineralogy of the samples (Figure 6.42). | 6-35 |
| Table 6.12: Summary of observations from FESEM images and the mineralogy of the samples (Figure 6.42). | 6-56 |
| Table 6.13: Observation and properties of Ti and TiO ₂ that affect the cell | 6-57 |
| Table 7.1: Gelation treatment conditions for all samples. | 7-2 |

| | | |
|-------------|--|------|
| Table 7.2: | The mineralogy (GAXRD) of films produced from gel oxidation (without stirring; A = anatase; R = rutile; N = sodium titanate). | 7-8 |
| Table 7.3: | Features observed from the FESEM images shown in Figures 7.7 - 7.10. | 7-14 |
| Table 7.4: | Observation of hydroxyapatite formation in SBF on the surface of titanium after gelation and oxidation at 400°, 600°, and 800°C. | 7-37 |
| Table 7.5: | Minerals and comparative amounts detected by XRD on the surface of titanium after gelation and oxidation of Ti without UV irradiation. | 7-37 |
| Table 7.6: | Scratch hardness results. | 7-38 |
| Table 7.7: | Summary of observations from FESEM images and mineralogy of the samples shown in Figure 7.22. | 7-40 |
| Table 7.8: | Gelation treatment and nomenclature for all samples. | 7-41 |
| Table 7.9: | Summary of observations from GAXRD patterns of the samples (Figures 7.23 to 7.26). | 7-42 |
| Table 7.10: | Published Raman microspectroscopy data. | 7-48 |

CHAPTER 1

INTRODUCTION

Titanium and its alloys have been used widely in biomedical implants and dental applications for their excellent biocompatibility, superior mechanical properties, and corrosion resistance. These materials are used for the repair and reconstruction of damaged parts of the body, including replacements for hips, knees, teeth, and fixators for fractured bones.

In biomaterial applications, some general terms (Table 1.1) such as *toxic*, *bioinert*, *bioactive*, and *bioresorbable* are used to classify the material's tissue response [1]. Titanium is considered to be *non-bioactive* for implants in bones.

Table 1.1: Type of implant - tissue response [1].

| Material | Explanation | Tissue Response | Examples |
|-----------------|--|--|---|
| Toxic | Material is toxic | The surrounding tissue dies | Copper |
| Bioinert | Material is non-toxic and biologically inactive | A fibrous tissue of variable thickness forms | Alumina, zirconia, titania, titanium and its alloys |
| Bioactive | Material is non-toxic and biologically active | An interfacial bond forms, between the tissue and material | Hydroxyapatite, bioactive glasses |
| Bioresorbable | Material is non-toxic and dissolves in surrounding environment | The surrounding tissue replaces it. | Tri-calcium phosphate |

For further improvement in biocompatibility, oxide surface modifications of titanium have been investigated. This is particularly relevant as all metallic titanium implants have a thin passivating oxide layer, so, in the past, these would have been implanted without the knowledge that the cellular response to the implant included the oxide component. Intentionally applied layers of titanium dioxide (TiO₂) produced by surface modification of titanium have emerged as important adjuncts to biomaterials owing to their excellent chemical and physical properties.

TiO₂ is known to have three natural polymorphs: rutile, anatase, and brookite [2]. Rutile, as the stable form of TiO₂ at ambient conditions, possesses unique semiconducting characteristics [3]. With regard to the chemical properties, anatase is an important phase since it is more reactive and thus more effective in forming apatite in simulated body fluid (SBF) [4]. It also is a more suitable form for photocatalytic activity than rutile [2]. Brookite normally is difficult to obtain during the ceramic processing [5].

Two methods, anodisation and gel oxidation, were used in the present work to form a titania layer on Ti substrates. Anodisation and gel oxidation are simple techniques that are useful at low temperature for producing TiO₂ layers on titanium substrates [6].

The TiO₂ layer on titanium was tested *in vitro* using simulated body fluid (SBF) using the method of Kokubo [4] and osteoblast bone-like cells. Previously, several researchers have conducted tests *in vitro* under normal conditions. However, no work has been carried out in the dark and under long-wave ultraviolet (UV) light, although TiO₂ is well known to react under ambient light. UV radiation can affect the TiO₂ implant surface, which is located near the skin (*e.g.*, dental implants and external bone-fracture fixator) and may change the properties of TiO₂ and its functions in the body in the long term.

CHAPTER 2

LITERATURE SURVEY

2.1 Titanium Dioxide (TiO₂)

Titanium dioxide (TiO₂) has been widely used in many industrial applications during the last few decades. Most of the applications are based on the special surfaces properties and catalytic properties. Due to these properties, TiO₂ has become the subject of many investigations for applications in optical, electrical and micro electronic, photonic, chemical and biomedical fields.

2.1.1 Uses

2.1.1.1 General Applications

TiO₂ is commonly used as a thin film and powder form. The general uses of TiO₂ are summarised in Table 2.1.

2.1.1.2 Photocatalysis

Over the past several years, several applications of photocatalytic technology have been examined. Some in use applications of photocatalysis are shown in Figure 2.1[7].

Table 2.1: The applications of TiO₂ in various fields.

| Application | Explanation / Applications | References |
|--|--|-------------------|
| White pigments | Used in paint, plastic, inks, paper, leather, textiles and cosmetic products | [7-11] |
| Metal oxide semiconductor field effect transistor (MOSFET) | High dielectric constants ($\epsilon = 100$) | [9,11,12] |
| Varistors | Used in ceramic and electric devices | [8] |
| Gas sensors | As humidity control To control the air/fuel mixture in car engines Utilized in determination of oxygen and CO at high temperatures (>600° C) | [8,9,11,13] |
| Biomaterials | Bone implant coatings As bone substituent As reinforcing mechanical support | [8,11] |
| Photo-assisted degradation of organic molecules | Purification of waste water Used in operating rooms in hospital Self-cleaning coating on car windshields | [7,8] |
| Anti cancer treatment | Photochemical treatment | [7] |
| As thin film optical interference coating | Antireflective coating Dielectric mirrors for lasers Metal mirrors with enhanced reflection Filters | [7,8,9,11] |
| As a protective coating | Corrosion resistant barriers | [8,9,13] |
| Photocatalysts (solar cells) | Used in the production of hydrogen and electric energy As anti-reflection coatings | [7,8,11,13] |
| Sunscreen | As UV absorber in sunscreen cream with high sun protection factors | [7,9,11] |
| Food | Foodstuff, food colouring (E-171) | [9,11] |
| Pharmaceuticals | As tablet coating, toothpastes | [9,11] |
| As catalysts | Selective reduction of NO _x to N ₂ , Hydrogen production by gas shift production, CO oxidation by O ₂ , H ₂ S oxidation to S, Reduction of SO ₂ to S by CO, NO ₂ storage | [9,11] |
| Used in fluxes and ceramics | Raw materials | [10] |
| Li-based batteries | Anatase form is used as anode material | [8,11] |
| Ultra-thin capacitors | | [9] |
| Electrochromic devices | Thin film coating | [8,13] |

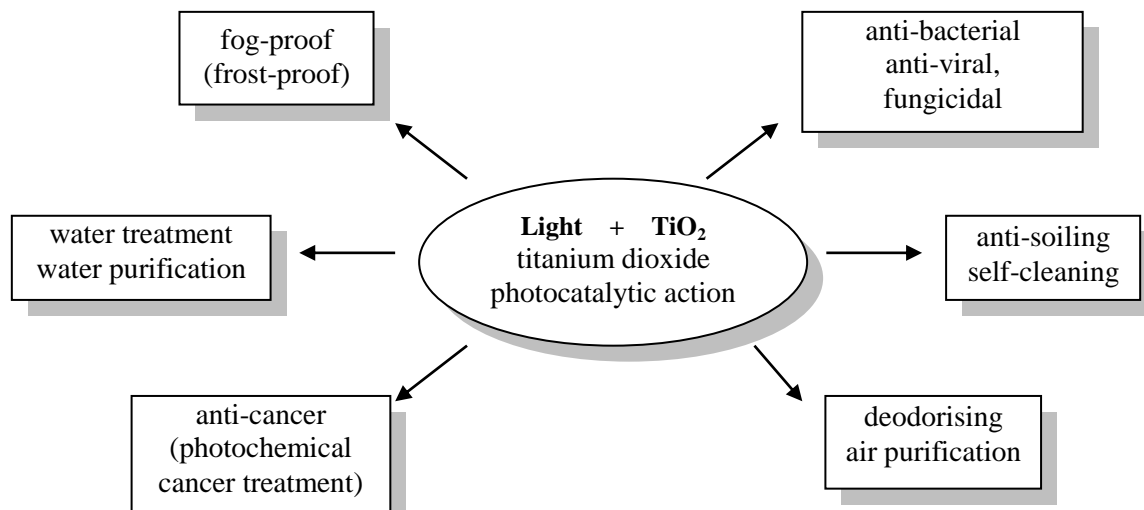


Figure 2.1: TiO_2 photocatalysis general applications [7].

Fujishima *et al.* [7] explained about the critical role of TiO_2 . By using TiO_2 in photocatalysis, the environment can be rendered clean and energy consumption can be decreased. Table 2.2 lists the various applications of TiO_2 as a photocatalysis [7].

Table 2.2: The applications of photocatalysis [7].

| Property/Function | Category | Applications |
|----------------------|--|---|
| Self-cleaning | Materials for residential and office buildings | Exterior tiles, kitchen and bathroom components, interior furnishings, plastic surfaces, aluminium siding, building stone and curtains, paper window blinds |
| | Indoor and outdoor lamps and related systems | Translucent paper for indoor lamp covers, coatings on fluorescent lamps and highway tunnel lamp cover glass |
| | Materials for roads | Tunnel wall, soundproofed wall, traffic signs and reflectors |
| | Others | Tent material, cloth for hospital garments and uniforms and spray coatings for cars |
| Air cleaning | Indoor air cleaners | Room air cleaner, photocatalyst-equipped air conditioners and interior air cleaner for factories |
| | Outdoor air purifiers | Concrete for highways, roadways and footpaths, tunnel walls, soundproof walls and building walls |
| Water purification | Drinking water | River water, ground water, lakes and water-storage tanks |
| | Others | Fish feeding tanks, drainage water and industrial wastewater |
| Anti tumour activity | Cancer therapy | Endoscopic instruments |
| Self-sterilising | Hospital | Tiles to cover the floor and walls of operating rooms, silicone rubber for medical catheters and hospital garments and uniforms |

2.1.1.3 Biomedical Applications

TiO₂ is used in biomedical applications as fine particles, coatings and oxide films on the outer surface of biomaterials (Table 2.3). The surface of the Ti-based alloys forms TiO₂ layers in aqueous solutions in the human body and act as the interface for strong bonding with natural connective tissue [14]. The TiO₂ film also provides corrosion resistance and contributes to improve biocompatibility of the implant [8].

Fujishima *et al.* [15] implanted cancer cells under the skin of mice to cause tumours to form, and when the size of the tumours grew to about 0.5 cm, suspension containing fine particles of titanium dioxide was injected into it. After 3 days, the skin was cut open to expose the tumour and it was irradiated with ultraviolet (UV) and thus treatment clearly inhibited the tumour growth. However, this technique was not effective in stopping cancer which had grown beyond a certain size limit [15].

Table 2.3: Applications of TiO₂ in biomedical fields.

| Form | Application / Explanations | References |
|-------------------|---|------------|
| Films on Metallic | Oral implants <i>Endosteal implants</i> <i>Implant retained suprastructure</i> <i>Combined denture</i> | [8,16-18] |
| | Orthopaedic implants <i>Hip joint implants</i> <i>Knee joint implants</i> <i>Bone-fracture fixation (screws and plates)</i> <i>External bone-fracture fixation</i> | [8,16,17] |
| Films on Polymers | Contact lenses | [7] |
| | Catheters | [7] |
| Powders | Cancer treatment <i>HeLa (cancer cells)</i> | [7] |
| | Pathogenic organism photodegradation <i>Escherichia coli</i> <i>U 937 -Ten and 30 min of illumination in the presence of TiO₂ leads to 80% and complete killing of human U 937 monocytic leukaemia cells</i> | [11] |

2.1.2 Crystal Structure and Phase Transformation

Titanium forms four well-defined oxides; monoxide (TiO), sesquioxide (Ti₂O₃), dioxide or titanic acid (TiO₂) called titania and pentoxide (Ti₃O₅) as shown in Figure 2.2. There are many differences in structural and chemical properties between its oxides

(Table 2.4). From a practical standpoint, the dioxide (TiO_2) is the most important oxide [19].

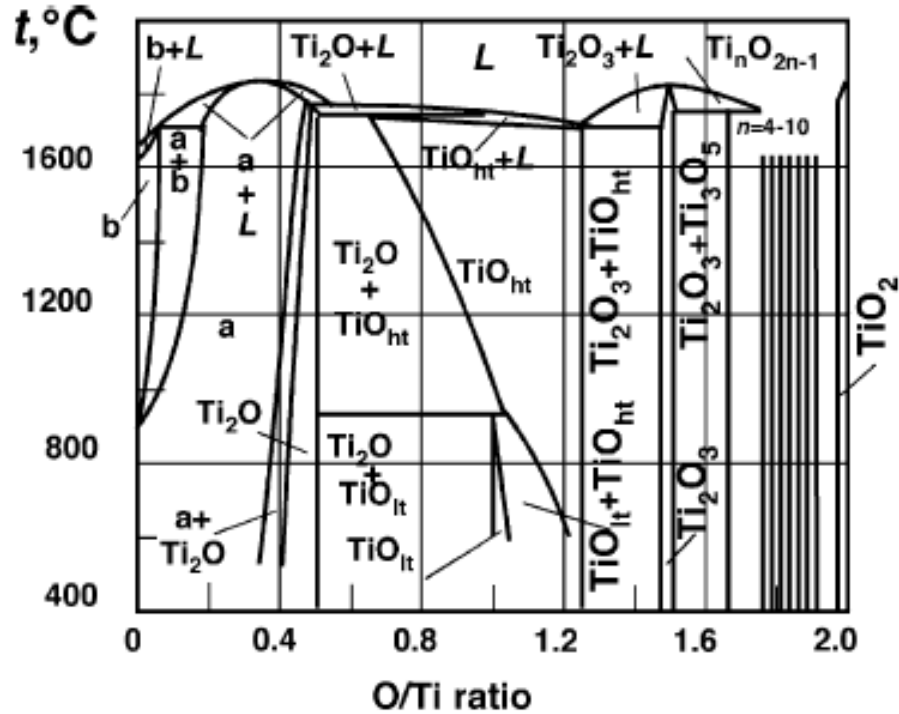


Figure 2.2: Phase diagram of the Ti-O system taken from Samsonov [20]. The region $\text{Ti}_2\text{O}_3 - \text{TiO}_2$ contains Ti_2O_3 , Ti_3O_5 , seven discrete phases of the homologous series $\text{Ti}_n\text{O}_{2n-1}$ (Magneli phases) and TiO_2 [8].

TiO_2 exists in nature in the form of minerals like anatase, brookite and rutile. Rutile is commonly found in nature; however, anatase and brookite are extremely rare. Generally, TiO_2 exist in an amorphous form at temperature below 350°C [9]. Above that temperature, anatase phase is formed and at temperatures greater than about 800°C , the most stable crystalline phase rutile, is formed [9,21].

According to Bokhimi [22], in most cases of TiO_2 synthesis, anatase is the main phase and brookite occurs as a minority phase, depending on synthesis conditions. The rutile phase is obtained by annealing anatase and brookite at temperature higher than 500°C [22]. The crystal structures of the three oxide forms can be discussed further in terms of orientation of the (TiO_2^6) octahedral [11].

Table 2.4: Properties of titanium oxides at various oxidation states [12,23].

| Property | TiO ₂ | | | TiO | Ti ₂ O ₃ |
|-----------------------------------|------------------|------------|------------|--------|--------------------------------|
| | brookite | anatase | rutile | | |
| Colour | dark brown | white | white | bronze | purple-violet |
| Melting point, °C | - | - | 1830-50 | 1737 | 2127 |
| Density (25°C), kg/m ³ | 4170 | 3900 | 4270 | 4888 | 4486 |
| Crystal structure | orthorhombic | tetragonal | tetragonal | Cubic | rhombohedral [24] |

2.1.2.1 Anatase

Anatase which refers to the long vertical axis, was named by R.J. Haüy in 1801 from the Greek word ‘anatisis’ meaning ‘extension’ [11]. Anatase has a tetragonal crystalline structure (Figure 2.3a) [22] and is built up from octahedra that are connected at their edge (Figure 2.3b) [11].

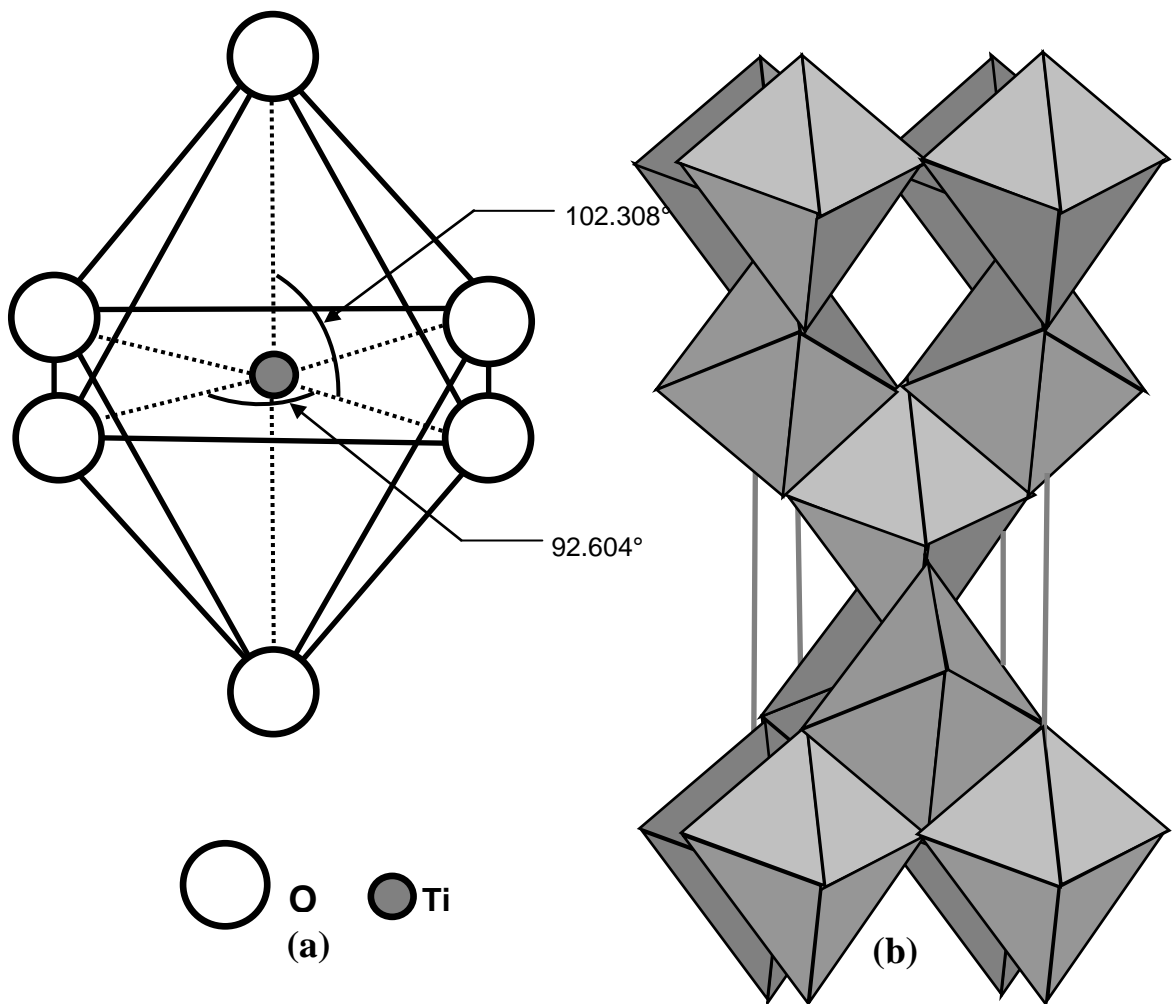


Figure 2.3: Crystal structure of anatase [8,11,22].

2.1.2.2 Rutile

Rutile was discovered by Werner in Spain in 1803. Its name is derived from the Latin 'rutilus' meaning red. Rutile is the most stable form of TiO_2 [11]. Rutile has a crystal structure with tetrahedral symmetry (Figure 2.4a) [22]. Rutile is built up from octahedra that are connected predominantly at their edges (Figure 2.4b) [11].

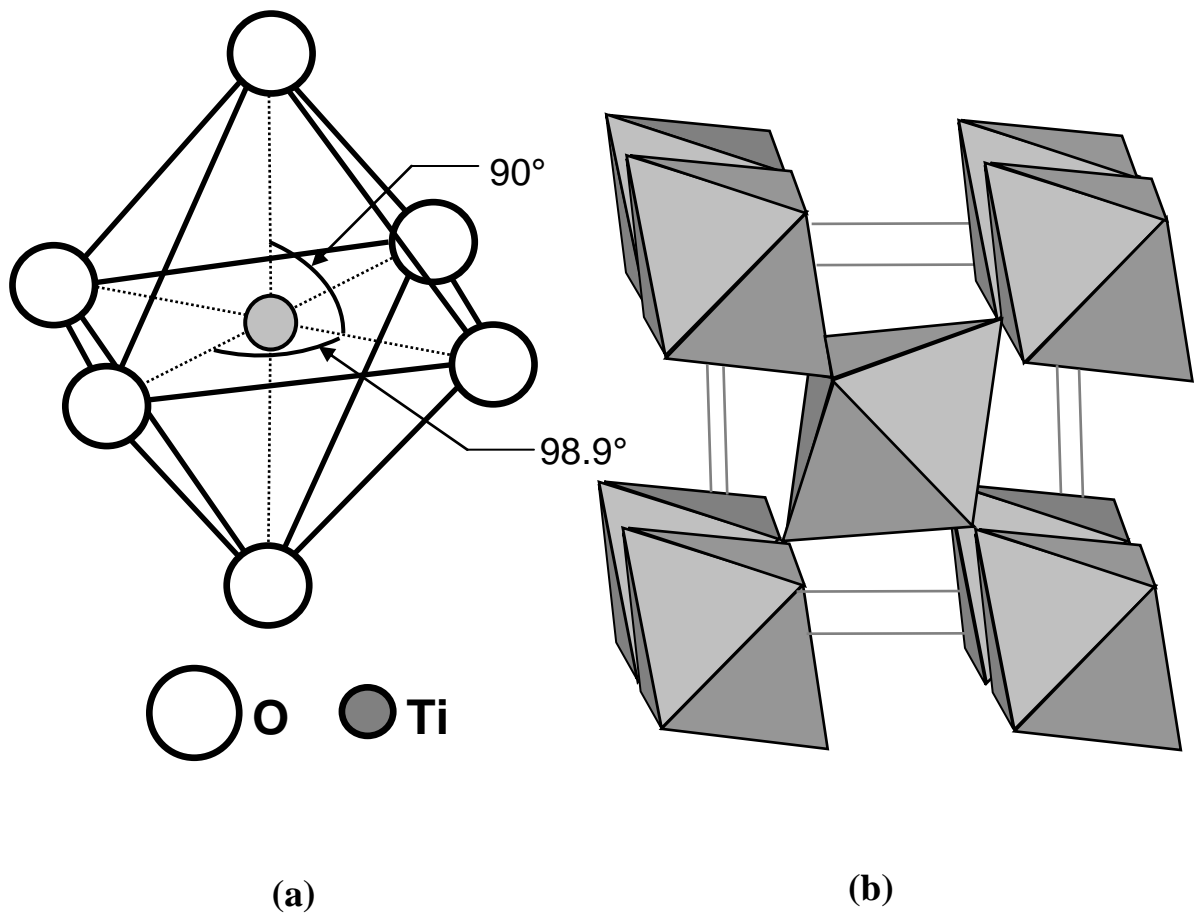


Figure 2.4: Crystal structure of rutile [11,22].

2.1.2.3 Brookite

Brookite was discovered by A. Levy in 1825 at Snowen (Pays de Gales, England) and it was named in honour of the English mineralogist, H.J. Brooke [11]. Brookite has an orthorhombic crystalline structure. The crystal structure can be described as distorted octahedra with a titanium atom the centre and oxygen atoms in the vertices (Figure 2.5a) [22]. Brookite is built up from the octahedra that are connected at their corner and edges (Figure 2.5b) [11].

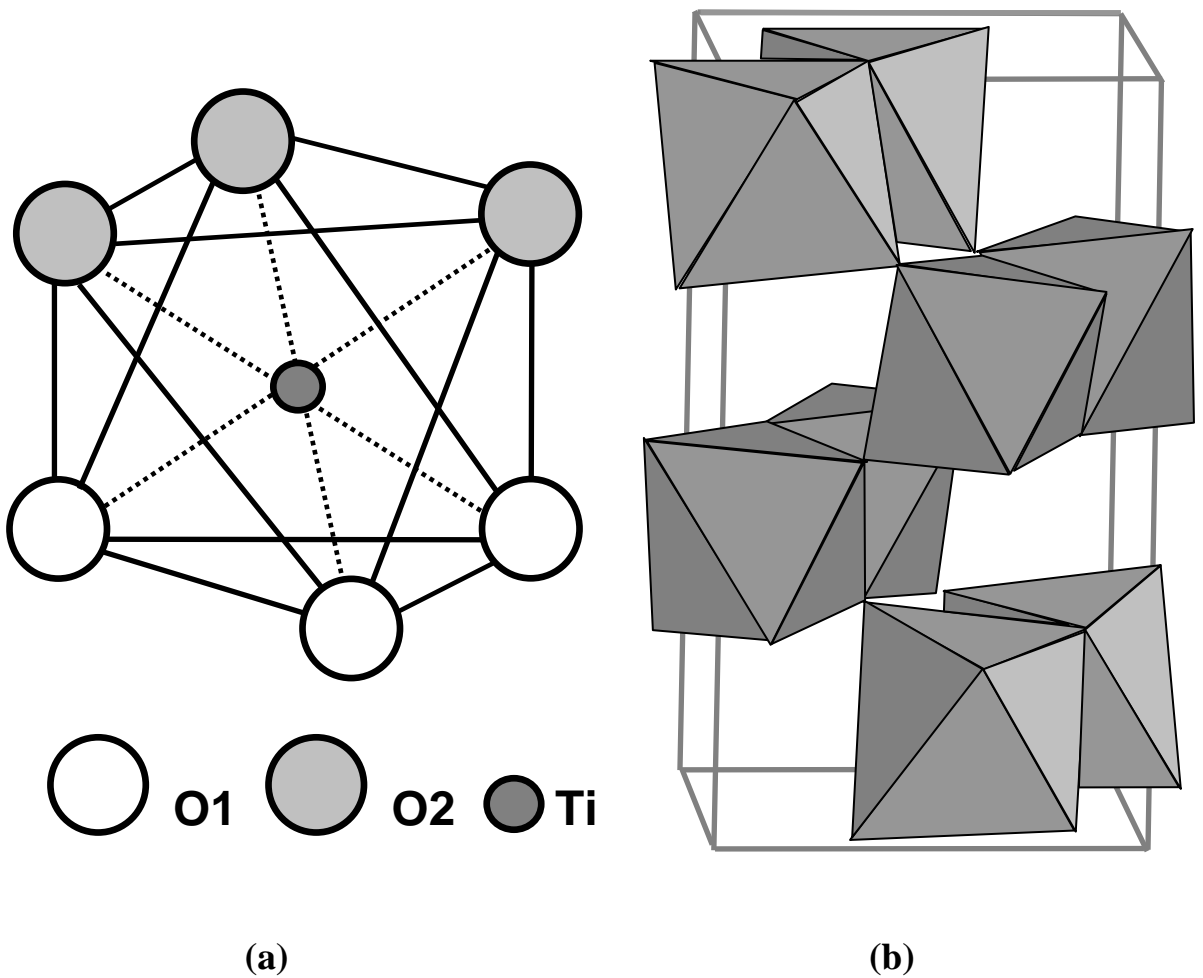


Figure 2.5: Crystal structure of brookite [11,22].

2.1.3 Thermodynamics and Phase Equilibrium

The thermodynamic phase stability in the Ti-O system is calculated based on calorimetric data [11]. Based on minor differences in the Gibbs free energy (4-20 kJ/mole) value between the three phases, the most stable phase is believed to be rutile at normal pressure and temperatures as compared to the other two phases. Particle size is also known affect to the phase stability due to its association with surface energy and surface stress. Thermodynamically, anatase is most stable at sizes less than 11 nm, brookite between 11 and 35 nm, and rutile at sizes greater than 35 nm. The transformation of anatase into rutile at room temperature is very slow and practically does not occur. At macroscopic scale, the transformations of bulk TiO₂ occur at temperatures more than 600°C.

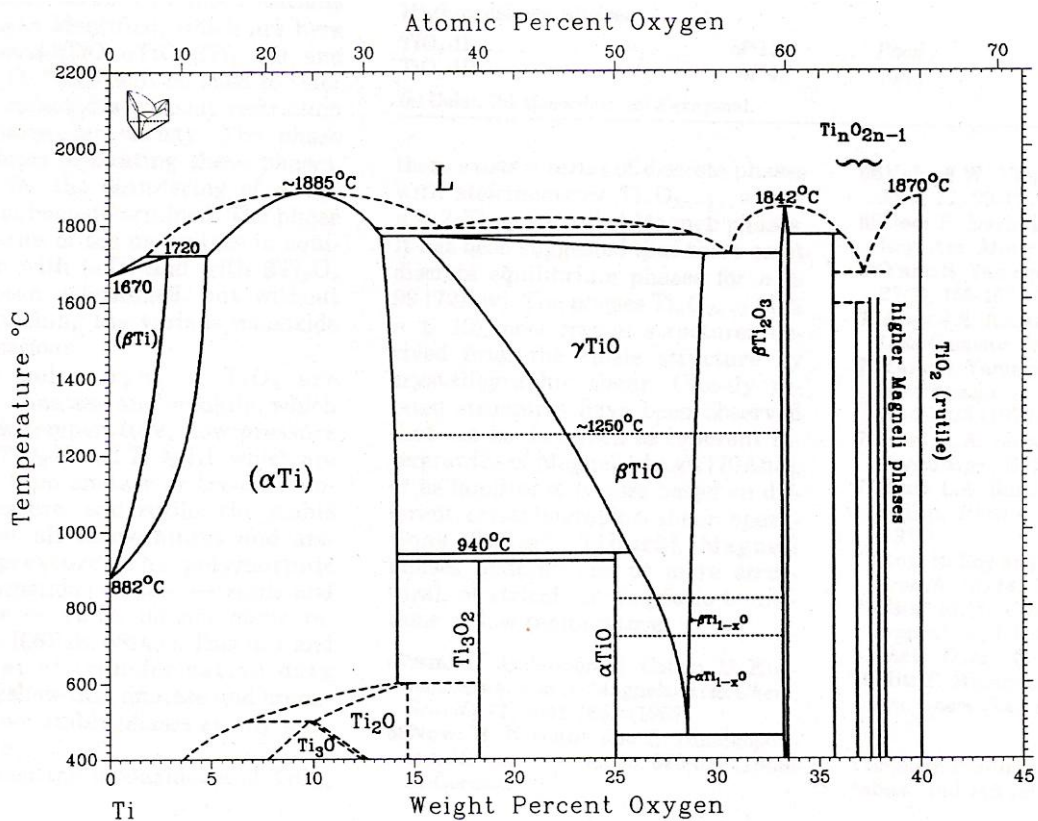


Figure 2.6: Ti-O phase diagram [25].

The phase equilibria and crystal structures of the Ti-O system range between pure Ti and TiO₂ as shown in Figure 2.6. High solubility of oxygen in titanium (α Ti) at low temperature leads to formation of Ti₂O, Ti₃O and possibly Ti₆O. Ti₂O has the anti-CdI₂ structure with alternate oxygen layers vacant and additional vacancies randomly distributed in occupied layer [26-29]. Monoxides (γ TiO at high temperature)

structures are based on the NaCl structure. Four modifications of TiO have been identified, α TiO, β TiO, α Ti_{1-x}O, and β Ti_{1-x}O [25]. The special points of the Ti-O phase diagram are summarised in Table 2.5 and Table 2.6.

Table 2.5: The special points of the Ti-O phase diagram [25].

| Phase | Composition, at % O | | | Temperature (°C) | Reaction type |
|---|---------------------|-------|-------|------------------|---------------------------|
| | | | | | |
| L + (α Ti) \leftrightarrow (β Ti) | 5 | 13 | 8 | 1720 \pm 25 | Peritectic |
| L \leftrightarrow (α Ti) | | ~24 | | 1885 \pm 25 | Congruent Melting |
| (α Ti) + Ti ₃ O ₂ \leftrightarrow Ti ₂ O | 33.3 | 40 | 33.9 | ~600 | Peritectoid |
| (α Ti) + Ti ₂ O ₃ \leftrightarrow Ti ₃ O | ~17 | ~25 | ~24.5 | ~500 | Peritectoid |
| L \leftrightarrow (α Ti) + L | ~37 | ~31 | ~53 | ~1800 | Monotectic (?) |
| L + (α Ti) \leftrightarrow γ TiO | ~55 | 31.4 | 34.5 | 1770 | Peritectic |
| γ TiO \leftrightarrow β TiO | | - | | ~1250 | Unknown |
| β TiO \leftrightarrow β Ti _{1-x} O | | - | | | Unknown |
| β Ti _{1-x} O \leftrightarrow α Ti _{1-x} O | | - | | | Unknown |
| (α Ti) + β TiO \leftrightarrow α TiO | 33.3 | 51 | 50 | 940 | Peritectoid |
| (α Ti) + α TiO \leftrightarrow Ti ₃ O ₂ | 32.4 | 50 | 40 | 920 | Peritectoid |
| α Ti _{1-x} O \leftrightarrow α TiO + β Ti ₂ O ₃ | 54.5 | 50 | 60 | 460 | Eutectoid |
| L \leftrightarrow γ TiO + β Ti ₂ O ₃ | ~57 | 54.5 | 59.8 | 1720 | Eutectic |
| L \leftrightarrow β Ti ₂ O ₃ | | 60 | | 1842 | Congruent |
| L + β Ti ₂ O ₃ \leftrightarrow β Ti ₃ O ₅ | 63 | 60.2 | 62.5 | 1770 | Peritectic |
| β Ti ₂ O ₃ \leftrightarrow α Ti ₂ O ₃ | | 60 | | ~180 | Unknown |
| β Ti ₃ O ₅ \leftrightarrow α Ti ₃ O ₅ | | 62.5 | | 187 | Unknown |
| γ Ti ₄ O ₇ \leftrightarrow β Ti ₄ O ₇ | | 63.64 | | -123 | Unknown |
| β Ti ₄ O ₇ \leftrightarrow α Ti ₄ O ₇ | | 63.64 | | -148 | Unknown |
| L \leftrightarrow β Ti ₃ O ₅ + ? | ~64 | 62.5 | - | ~1670 | Eutectic |
| β Ti ₃ O ₅ + β Ti ₅ O ₉ \leftrightarrow γ Ti ₄ O ₇ | 62.5 | 64.29 | 63.64 | ~1500 | Peritectoid |
| L \leftrightarrow TiO ₂ | | 66.7 | | 1870 | Congruent |
| L \leftrightarrow (β Ti) | | 0 | | 1670 | Melting point |
| (β Ti) \leftrightarrow (α Ti) | | 0 | | 882 | Allotropic transformation |

There are five polymorphs of TiO₂ that are anatase, brookite, TiO₂-II, TiO₂-III and rutile. Anatase and brookite are formed at low temperature and low pressure; TiO₂-II and TiO₂-III are formed from anatase or brookite under high pressure; and rutile is the stable phase at room temperature and pressure. The polymorphic transformations anatase \rightarrow rutile and brookite \rightarrow rutile do not occur reversibly [30,31]. The magneli phases are a series of discrete phases with stoichiometry Ti_nO_{2n-1} where $n \geq 2$. The magneli phases exist in between the monoxides (TiO) and dioxide (TiO₂). Roy and White have suggested that there exists discrete equilibrium phases for $n \leq 99$ [32]. The

phases Ti_nO_{2n-1} ($4 \leq n \leq 10$) have crystal structures derived from the rutile structure by crystallographic shear [25].

Table 2.6: Ti-O crystal structure data [25].

| Phase | Composition, at % O | Pearson symbol | Space group | Structure-bericht designation | Prototype |
|--|---------------------|----------------|---------------------------------------|-------------------------------|---|
| (β Ti) | 0 to 8 | <i>cI2</i> | <i>Im3m</i> | A2 | W |
| (α Ti) | 0 to 31.9 | <i>hP2</i> | <i>P6₃/mmc</i> | A3 | Mg |
| Ti ₃ O | ~20 to ~30 | <i>hp</i> ~ 16 | <i>P⁻31c</i> | - | - |
| Ti ₂ O | ~25 to 33.4 | <i>hP3</i> | <i>P⁻3m1</i> | - | Anti-CdI ₂ |
| γ Ti | 34.9 to 55.5 | <i>cF8</i> | <i>Fm3m</i> | B1 | CINa |
| Ti ₃ O ₂ | ~40 | <i>hP</i> ~ 5 | <i>P6/mmm</i> | - | - |
| β TiO | - | (a) | - | - | - |
| α TiO | ~50 | <i>mC16</i> | A2/m or B [*] / [*] | - | - |
| β Ti _{1-x} O | ~55.5 | <i>oI12</i> | <i>I222</i> | - | - |
| α Ti _{1-x} O | ~55.5 | <i>tI18</i> | <i>I4/m</i> | - | - |
| β Ti ₂ O ₃ | 59.8 to 60.2 | <i>hR30</i> | <i>R⁻3i</i> | D5 ₁ | α Al ₂ O ₃ |
| α Ti ₂ O ₃ | 59.8 to 60.2 | <i>hR30</i> | <i>R⁻3c</i> | D5 ₁ | α Al ₂ O ₃ |
| β Ti ₃ O ₅ | 62.5 | (b) | - | - | Anosovite |
| α Ti ₃ O ₅ | 62.5 | <i>mC32</i> | <i>C2/m</i> | - | - |
| α' Ti ₃ O ₅ | (a) | <i>mC32</i> | <i>Cc</i> | - | V ₃ O ₅ |
| γ Ti ₄ O ₇ | 63.6 | <i>aP44</i> | <i>P⁻1</i> | - | - |
| β Ti ₄ O ₇ | 63.6 | <i>aP44</i> | <i>P⁻1</i> | - | - |
| α Ti ₄ O ₇ | 63.6 | <i>aP44</i> | <i>P⁻1</i> | - | - |
| γ Ti ₅ O ₉ | 64.3 | <i>aP28</i> | <i>P⁻1</i> | - | - |
| β Ti ₆ O ₁₁ | 54.7 | <i>aC68</i> | <i>A⁻1</i> | - | - |
| Ti ₇ O ₁₃ | 65.0 | <i>aP40</i> | <i>P⁻1</i> | - | - |
| Ti ₈ O ₁₅ | 65.2 | <i>aC92</i> | <i>A⁻1</i> | - | - |
| Ti ₉ O ₁₇ | 65.4 | <i>aI52</i> | <i>P⁻1</i> | - | - |
| Rutile | ~66.7 | <i>tP6</i> | <i>P4₂/mnm</i> | C4 | Rutile |
| Metastable phase | | | | | |
| Anatase | - | <i>tI12</i> | <i>I4₁/amd</i> | C5 | Anatase |
| Brookite | - | <i>oP24</i> | <i>Pbca</i> | C21 | Brookite |
| High pressure phase | | | | | |
| TiO ₂ -II | - | <i>oP12</i> | <i>Pbcn</i> | - | α PbO ₂ |
| TiO ₂ -III | - | ~ <i>hP48</i> | (c) | - | - |

(a) Cubic, (b) Monoclinic, (c) Hexagonal

2.1.4 Properties of TiO₂

The physical, optical, electrical and chemical properties of TiO₂ depend greatly on the amorphous or crystalline phase of the material [9]. The bulk properties of TiO₂ are shown in Table 2.7.

Table 2.7: Bulk properties of the three main polymorphs TiO₂ (anatase, brookite and rutile) [8].

| Property | TiO ₂ | | |
|--|----------------------|--------------------------|--------------------------|
| | brookite | anatase | rutile |
| Space group | D_{2h}^{15} $Pbca$ | D_{4h}^{19} $I4_1/amd$ | D_{4h}^{14} $P4_2/mnm$ |
| Lattice constant (nm) | | | |
| a | 0.5346 | 0.3733 | 0.4584 |
| b | 0.9166 | - | - |
| c | 0.5135 | 0.9370 | 0.2953 |
| c/a | 0.944 | 2.51 | 0.644 |
| Standard heat capacity, C_p^o , 298.15 J/(mol °C) | - | 55.52 | 55.06 |
| Electron mobility, μ (cm ² /Vs) | - | ~10 | ~1 |
| Band gap (eV) | - | 3.2 | 3.0 |
| Refractive index | | | |
| n_g | 2.809 | 2.5688 | 2.9467 |
| n_p | 2.677 | 2.6584 | 2.6506 |

2.2.4.1 Physical Properties

The physical properties of TiO₂ depend on the amorphous or crystalline nature of the material. Amorphous TiO₂ has voids and relatively low density and does not have a crystallographic structure. The amorphous TiO₂ phase can be produced at low temperature 100°C – 150°C as a thin film deposit on substrates. However, TiO₂ thin films that are produced by chemical reaction form anatase at the lowest temperatures [9].

TiO₂ has three crystalline phases. In thin films, normally anatase and rutile are observed. Polycrystalline anatase film can be obtained from amorphous TiO₂ film by annealing at higher temperatures [9]. The transition from amorphous to crystalline anatase film occurs at ~ 300 – 365°C and from anatase to rutile occurs at ~ 700 – 1100°C. Both anatase and rutile have tetragonal crystallographic structure but rutile is more densely packed and thus denser than anatase. Amores *et al.* [33] have explained in detail about the phase transformation from anatase to rutile in the high temperature sintering process as shown in Figure 2.7. The proposed mechanism for the sintering and transformation of anatase into rutile comprises on:

1. The smallest particles coalesce, forming bigger particles.
2. The fractions of particles that are already large have been shown not to undergo sintering.
3. Heat evolved from the exothermic sintering process causes the local nucleation of rutile.
4. The conversion to rutile is also an exothermic process, leading to the transformation of the whole particle to rutile.

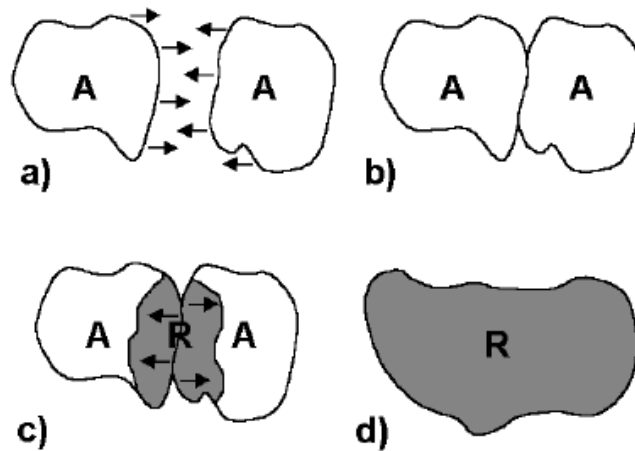


Figure 2.7: Proposed mechanism for the sintering and transformation of anatase into rutile. (adapted from [33]).

Anatase and rutile have different densities due to different packing arrangement. Table 2.8 shows the density of the various phases and thin films mentioned by Richards [9]. Density of TiO_2 thin film can be calculated by using the equation derived from the linear relationship between density and refractive index (Figure 2.8) [34].

Table 2.8: Various density of TiO_2 [9].

| Structure | Density (kg/m^3) | Notes | References |
|-----------|-----------------------------|--|------------|
| Amorphous | 2400 | Porous film | [35] |
| | 3200 -3650 | Typical value | [36] |
| | 3600 -3800 | Films deposited with a high kinetic energy | [34] |
| Brookite | 4170 | Bulk | [8] |
| Anatase | 3900 | Bulk | [8] |
| | 3840 | | [9] |
| Rutile | 4270 | Bulk | [8] |
| | 4260 | | [9] |
| | 4090-4100 | Thin film | [34,37] |

The equation of line in Figure 2.7 is

$$n_f = 0.42751\rho + 0.91933 \quad (2.1)$$

$$\rho = \frac{n_f - 0.91933}{0.42751} \quad (2.2)$$

where ρ and n_f are the TiO₂ film density (kg/m³) and refractive index respectively. The porosity of the thin film can be determined using equation 2.3 [38].

$$\text{Porosity} = \frac{n_b^2 - 1}{n_f^2 - 1}, \quad (2.3)$$

where n_b is the refractive index of the bulk single crystal material. This value is an approximation due to the fact that firstly, both anatase and rutile crystals exhibit strong birefringence and secondly mixed anatase / rutile phases can exist [9].

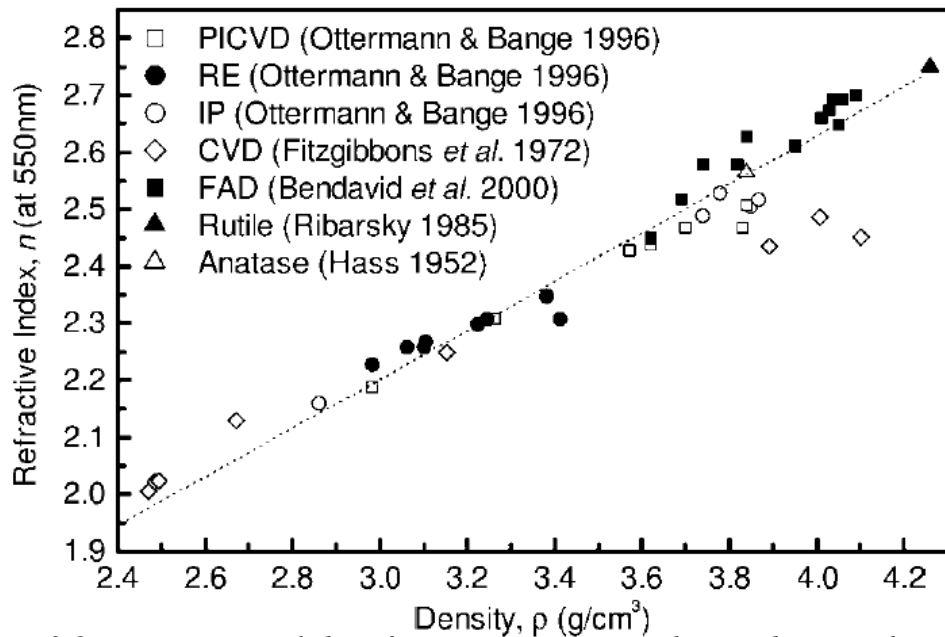


Figure 2.8: Experimental data from previous researchers indicating that a linear correlation between TiO₂ film density and refractive index is observed over for a wide range of values. Ottermann and Bange [39], Fitzgibbons *et al.* [40], Bendavid *et al.* [34], Hass [41], and Ribarsky [42] were used. (Adapted from [34]).

2.2.4.2 Chemical Properties

TiO₂ is relatively inert and has good corrosion resistance in a biological environment. TiO₂ film on titanium and titanium based alloys is widely used in biomedical and dental applications [43]. It exhibits stability and corrosion resistance that protects the metal

from further oxidation in vitro. When in contact with body fluids that have pH values close to neutral, the materials show corrosion rates that are extremely low and difficult to measure experimentally.

In general, crystalline phases of TiO₂, anatase and rutile are much more chemically resistant than amorphous TiO₂ [9]. Richard also found that amorphous TiO₂ films are highly soluble in hydrofluoric acid (HF), but dense and polycrystalline films are insoluble. The chemical resistance of TiO₂ to sulphuric acid (H₂SO₄) is very dependent on the film preparation technique [44], but TiO₂ is insoluble in all other concentrate acids and bases [9]. Barksdale reported that TiO₂ is slightly soluble in H₂SO₄, HF and a few strong alkalis, but it is almost completely chemically inert after annealing at 1000°C [19]. Strong basic solutions such as sodium hydroxide (NaOH) and ammonium hydroxide (NH₄OH) are used in etching processes for TiO₂ films [9].

2.2.4.3 Optical Properties

The important optical properties of TiO₂ are refractive index and extinction coefficient. Refractive index indicates the extent to which a light beam is reflected when passing through as compared to the vacuum substance. The refractive index of a TiO₂ thin film is less than that of anatase or rutile crystal. Anatase and rutile are birefringent crystals and their refractive indices are calculated using mean refractive index n_{mean} for a randomly oriented polycrystalline thin film (Equation 2.4).

$$n_{mean} = \frac{2n_{\perp} + n_{\parallel}}{3} \quad (2.4)$$

where $2n_{\perp}$ and n_{\parallel} are for oscillations perpendicular and parallel to the optical axis (axis of light can pass without undergoing double refraction), respectively [9]. The mean refractive indices for rutile and anatase (at $\lambda = 600$ nm) are 2.70 and 2.53 respectively [41,42].

Richard [9] presented information about the refractive index, optical bandgap and optical absorption in his work. The refractive indices for anatase single crystal from previous research and the rutile single crystal from Kim is shown in Figure 2.9. The

optical bandgap value of TiO_2 changes depending on its structure. The optical bandgap of amorphous TiO_2 is around 3.5 eV, while for anatase and rutile, it is about 3.2 eV and 3.05 eV, respectively. The optical absorption will increase with successive transformations from amorphous TiO_2 to anatase to rutile material. From Figure 2.10, anatase is seen to have an absorption edge with a lower steepness, which is attributed to the presence of excitons (bound state of an electron and a hole), and more imperfections and disorder than in anatase crystal. Figure 2.11 shows the exponential dependence of the absorption coefficient at 10 K for different polarisations when illuminated with UV light [9,45].

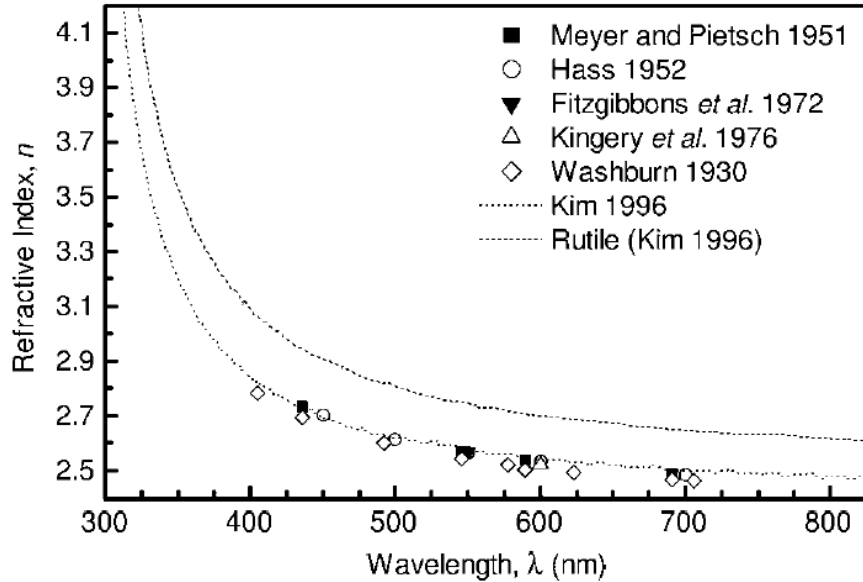


Figure 2.9: Published values for the refractive index of single crystal anatase, taken from Meyer and Pietsch [44]; Hass [41]; Fitzgibbons [40]; Kingery et al. [46]; Washburn [47] and Kim [48]. The dispersive curve for single crystal rutile from Kim is also given [48].

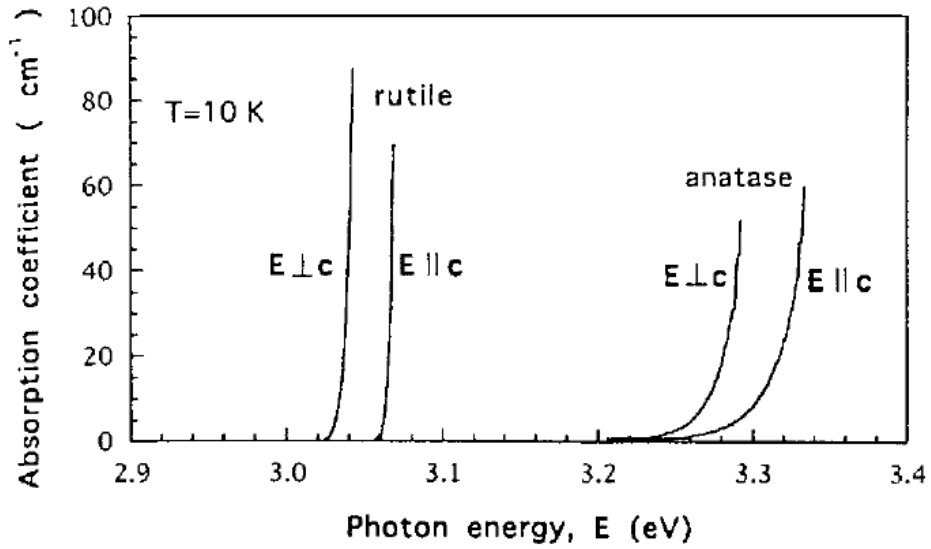


Figure 2.10: Fundamental absorption edge of anatase and rutile single crystal, measured at a temperature of 10 K (adapted from [45]).

The extinction coefficient k , play an attenuating role in the material. It is related to absorption coefficient α through this equation (Equation 2.5),

$$k = \frac{\alpha \lambda}{4\pi}, \quad (2.5)$$

where k and α are extinction coefficient and absorption coefficient, respectively [9]. Richard [9] also mentioned that the extinction coefficient of a film can be increased by scattering of light by surface and volume in imperfections, such as surface roughness, porous microstructure, and density fluctuations [9]. The term optical loss L is defined as

$$1 = R + T + L \quad (2.6)$$

with

$$L = A + S \quad (2.7)$$

where A is absorptance, S is the scattering component, R is reflectance and T is transmittance.

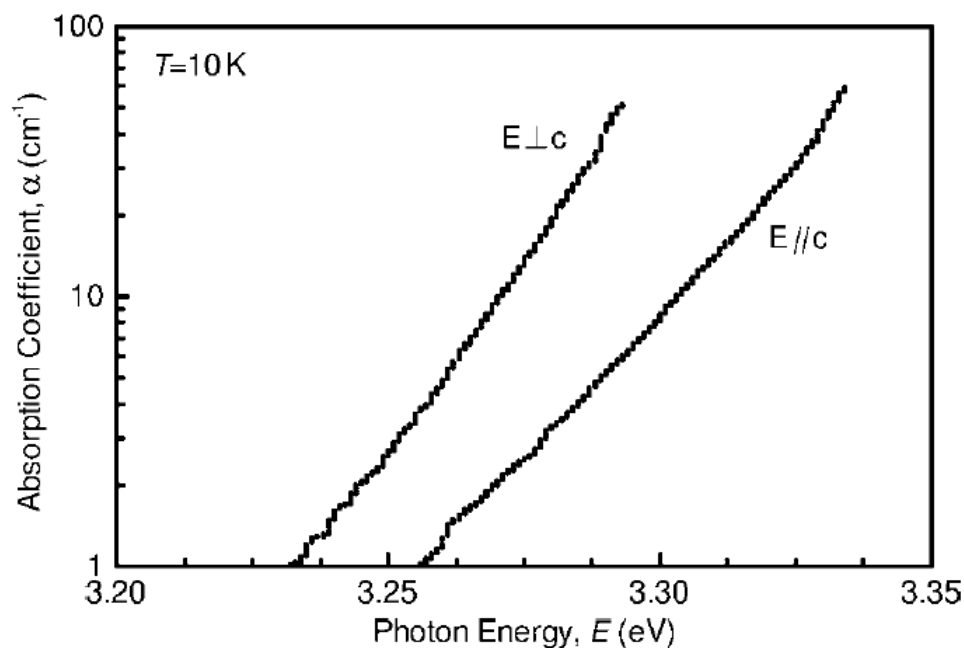


Figure 2.11: The exponential dependence of the absorption coefficient of single crystal anatase, measured at 10 K with light polarised in $E_{\perp c}$ and $E_{\parallel c}$ directions (adapted from [45]).

2.1.4.4 Photocatalytic Properties

The photocatalytic phenomenon has been studied extensively for several years by many researchers. Since TiO_2 is a semiconductor with a band gap of about 3.0 eV, UV light (with wavelengths shorter than ~ 400 nm) can excite pairs of electrons and holes [49]. The photogenerated electrons then react with molecular oxygen (O_2) to produce superoxide radical anions ($\bullet\text{O}_2^-$), and the photogenerated holes react with water to produce hydroxyl ($\bullet\text{OH}$) radicals. These two types of reactive radicals then work together to decompose organic compounds. The longer the film is illuminated with UV light, the more organic material that is decomposed, such that even an oily stain on the surface would gradually disappear under UV light [7]. Overall, the photocatalysed reaction may be summarized as follows:



Depending on the sign of the change in Gibbs free energy (ΔG°) value of the reaction (2.8), the semiconductor-sensitised reaction may be an example of photocatalysis or photosynthesis, respectively [11]. For a semiconductor photocatalyst to be efficient,

the different interfacial electron processes involving e^- and h^+ must compete effectively with the major deactivation processes involving $e^- - h^+$ recombination, which may occur in the bulk or at the surface (Figure 2.12). Ideally, a semiconductor photocatalyst should be chemically and biologically inert, photocatalytically stable, easy to produce and to use, efficiently activated by sunlight, able to efficiently catalyse reactions, cheap, and without risks for the environment or humans. Titanium dioxide (with sizes ranging from clusters to colloids to powders and large single crystals) is close to being an ideal photocatalyst, displaying almost all the above properties. The single exception is that it does not absorb visible light.

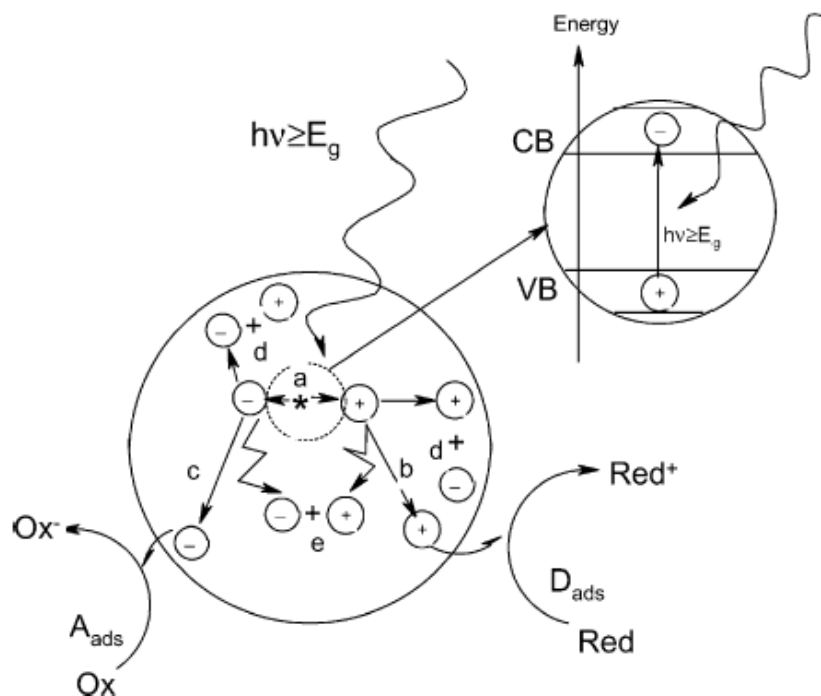


Figure 2.12: Major mechanism occurring on semiconductors: (a) electron-hole generation; (b) oxidation of donor (D); (c) reduction of acceptor (A); (d) and (e) electron-hole recombination at surface and in bulk, respectively [48].

Both crystal structures anatase and rutile, are commonly used as photocatalysts, with anatase showing greater photocatalytic activity for most reactions. It has been suggested that this increased photoreactivity is due to anatase having slightly higher Fermi level, lower capacity to adsorb oxygen and higher degree of hydroxylation (*i.e.*, number of hydroxy groups on the surface) [50]. Reactions in which both crystalline phases have the same photoreactivity or rutile having a higher one [51] have also been reported. Furthermore, there are also studies which claim that a mixture of anatase

(70–75%) and rutile (30–25%) is more active than pure anatase alone. The disagreement of the results may be due to the intervening effect of various coexisting factors, such as specific surface area, pore size distribution, crystal size, and preparation methods, or it may be related to the way the activity is expressed.

The behavior of Degussa P25 commercial TiO₂ photocatalyst, consisting of an amorphous state together with a mixture of anatase and rutile in an approximate proportion of 80/20, is observed to be more active than both the pure crystalline phases together [52]. The enhanced activity arises from the increased efficiency of the electron–hole separation due to the multiphase nature of the particles. Another commercial TiO₂ photocatalyst Sachtlebem Hombikat UV 100, consisting only of anatase, has a high photoreactivity due to fast interfacial electron-transfer rate. Water splitting is a special case, because band bending is necessary in order to oxidize water and large rutile particles (with a small surface area) are efficient [53].

2.2 Colour Properties of Titanium and TiO₂

2.2.1 Colour System

Colour is associated with visible light waves (wavelength distributions). Visible light is a very small part of electromagnetic energy; wavelengths within violet (400 nm) and red (700 nm) of the electromagnetic spectrum (Figure 2.13) [54,55]. The selective absorption of different amount of wavelengths within violet and red described as colour of objects. Wavelengths not absorbed are reflected or transmitted by objects and thus visible to observers [54].

The colour measurement for the scientific purpose is based on numerical representations or quantification of three colour response mechanisms in the human eye [54]. There are several methods of measurement:

- 1) RGB-based colour space
- 2) HSV and HLS colour space
- 3) CIE colour space

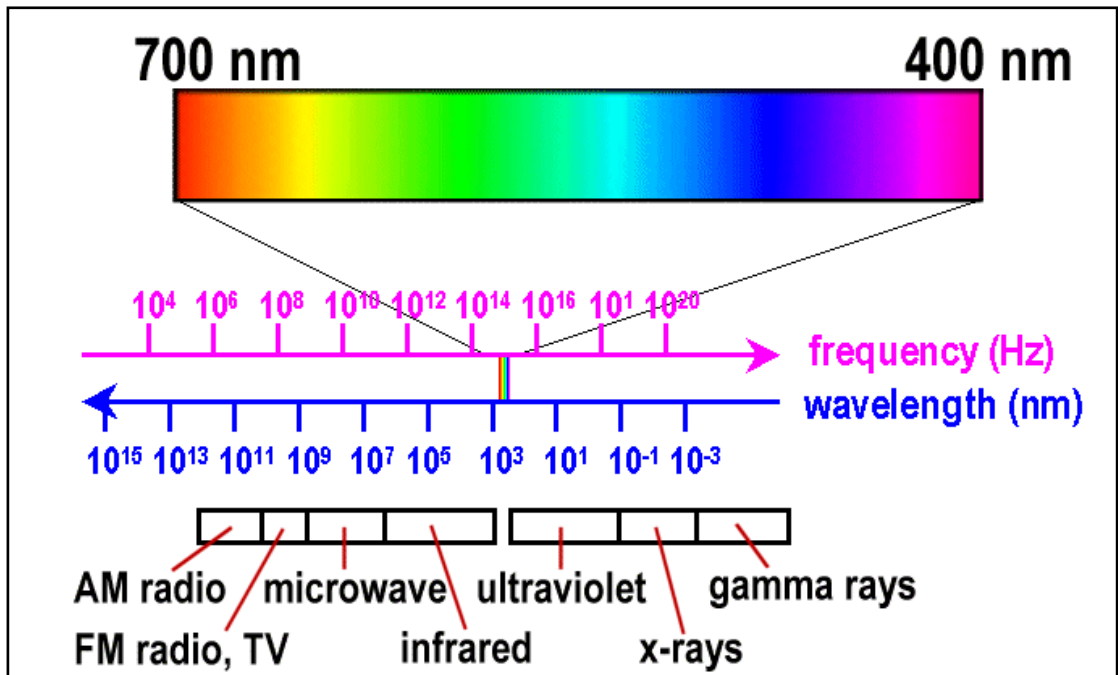


Figure 2.13: Visible light (wavelength, 400-700nm) as part of electromagnetic energy [55].

2.2.2 RGB-Based Colour Space

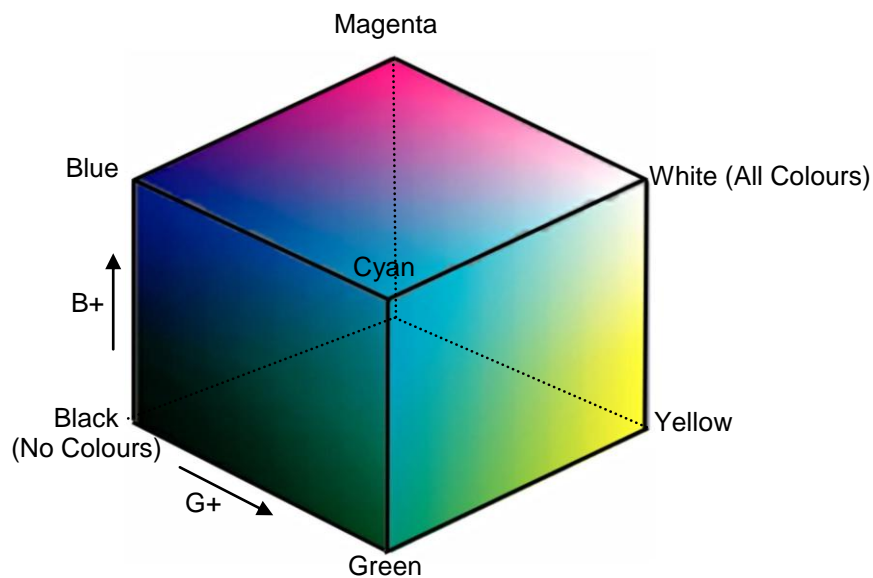


Figure 2.14: RGB space colour cube (Red corner is hidden from view)[55].

The most commonly used colour space is the RGB colour system (Figure 2.14). The RGB space is a three-dimensional colour cube with primary colour defined as (red,

green and blue), secondaries (cyan, magenta and yellow) and white. One corner of the cube is the origin for the RGB coordinate axes [56].

2.2.3 HSV and HLS Colour Space

A second colour space commonly used is the HSV and HLS colour space that are transformations of RGB. The name HSV stand for (hue-saturation-value is synonymous with HSB, hue-saturation-brightness), and HSL (hue-saturation-lightness) colour spaces. The two spaces can be described as being single and double cones respectively (Figure 2.15) [57].

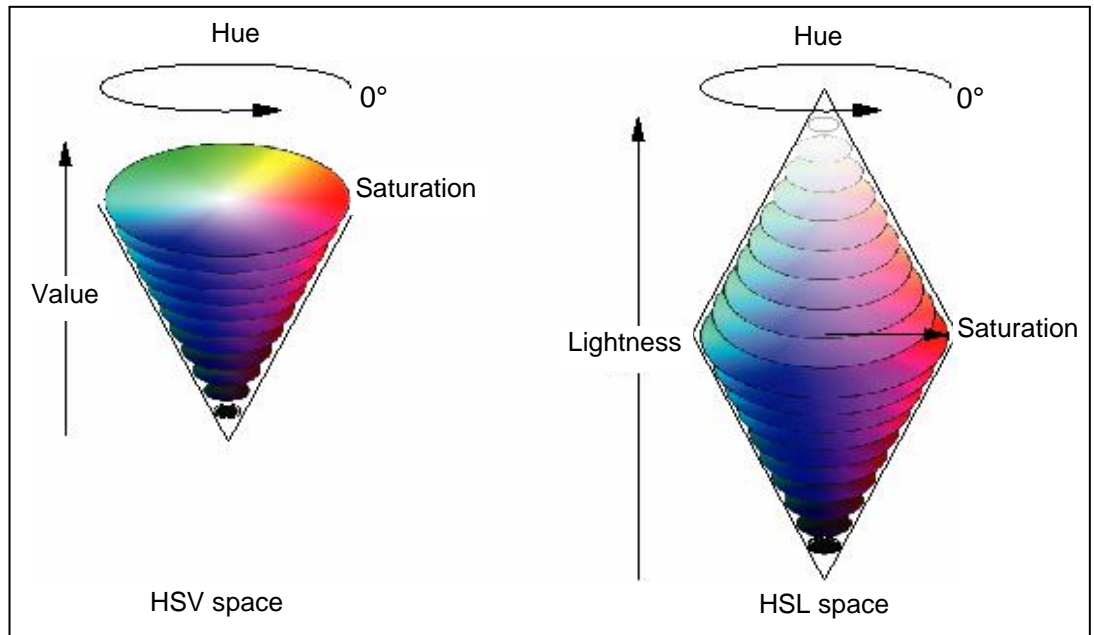


Figure 2.15: HSV and HSL colour space [55].

The components in HLS space are analogous, but not completely identical, to the components in HSV space. The hue component in both colour spaces is an angular measurement (represent by a disc). A hue value is indicated as in Table 2.9.

Table 2.9: Hue value and colours

| Primary colour | | Secondary colour | |
|----------------|-------|------------------|---------|
| 0° | red | 60° | yellow |
| 120° | green | 180° | cyan |
| 240° | blue | 300° | magenta |

The saturation component in both colour spaces describes colour intensity. A saturation value of 0 (in the middle of a disc) means that the colour is "colourless" (gray); a saturation value at the maximum (at the outer edge of a disc) means that the colour is at maximum "colourfulness" for that hue angle and brightness.

The value component in HSV describes the brightness. In both colour spaces, a value of 0 represents the absence of light, or black. In HSV space, a maximum value means that the colour is at its brightest. In HSL space, a maximum value for lightness means that the colour is white, regardless of the current values of the hue and saturation components [55]. Table 2.10 shows the difference between HSV and HSL system.

Table 2.10: The HSV (saturation and value) and HSL (saturation and lightness) [58]

| HSV | | | HSL | | |
|------------|-----|---------------|------------|-----|---------------------|
| Saturation | 0 | colourless | Saturation | 0 | colourless |
| | max | colourfulness | | 100 | Pure primary colour |
| Value | 0 | black | Lightness | 0 | black |
| | max | bright | | 100 | white |

According to Harold [54], scientific colour is measured based on numerical representations of the three colours that response to human eye. The human eye has receptors (called cone cells) for short (*S*), middle (*M*), and long (*L*) wavelengths. In 1931, The Commission Internationale de L'Éclairage (CIE) has defined a system to compute a triple of numerical components to be the mathematical coordinates of colour space and was called 1931 CIE XYZ colour space [59,54]. In the CIE XYZ colour space, the tristimulus values are called *X*, *Y*, and *Z*, which are roughly red, green and blue, respectively.

It is convenient to work in a 2D colour space. This is commonly done by projecting the 3D colour space onto the plane $X+Y+Z=1$, yielding a CIE chromaticity diagram (Figure 2.16).

The projection is defined as:

$$x = \frac{X}{X + Y + Z}$$

$$y = \frac{Y}{X + Y + Z}$$

$$z = \frac{Z}{X + Y + Z} = 1 - x - y$$

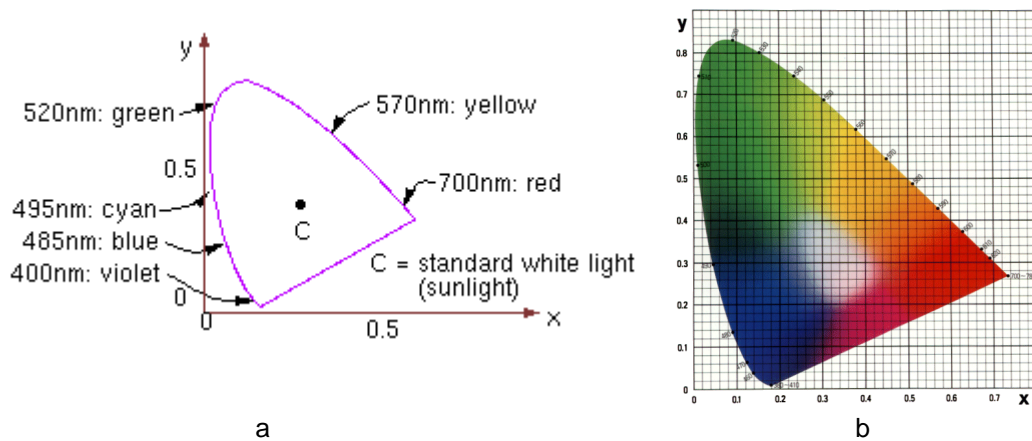


Figure 2.16: CIE chromaticity diagram, (a) schematic and (b) Colour [55].

2.2.4 Colour Measurement

Colour measurement by visual is subjective and difficult to correlate the observation of different observer. Scientific colour measurement is based on numerical representation due to difficulty to identify constantly, even for the same observer. Quantitative technique to measure colour are designed to be used as standard measurement.

The opponent-colours (L,a,b-type) colour scale are used in this study to measure the colour of the samples. The L,a,b-type scale original developed and refined by Richard S. Hunter between 1942 and 1958 [54]. In 1976, the CIE adopted another L,a,b-type

REFERENCES

- [1] L.L. Hench, "Bioceramics", *Journal of American Ceramic Society*, **81**, 1705-1728 (1998).
- [2] W. Payakgul, O. Mekasuwandumrong, V. Pavarajarna, and P. Praserthdama, "Effects of Reaction Medium on the Synthesis of TiO₂ Nanocrystals by Thermal Decomposition of Titanium (IV) n-butoxide", *Ceramics International*, **31**, 391-397 (2005).
- [3] H. Wua, X. Lua, B. Long, X. Wang, J. Wang, and Z. Jin, "The Effects of Cathodic and Anodic Voltages on the Characteristics of Porous Nanocrystalline Titania Coatings Fabricated by Micro Arc Oxidation", *Materials Letters*, **59**, 370-375 (2005).
- [4] T. Kokubo, H. M. Kim, and M. Kawashita, "Novel Bioactive Materials with Different Mechanical Properties", *Biomaterials*, **24**, 2161-2175 (2003).
- [5] A. Ravaglioli, and A. Krajewski, *Bioceramics: Materials, Properties, Application*, Chapman & Hall, London, 1992.
- [6] F. Xiao, K. Tsuru, S. Hayakawa, and A. Osaka, "In Vitro Apatite Deposition on Titania Film Derived from Chemical Treatment of Ti Substrates with an Oxysulfate Solution Containing Hydrogen Peroxide at Low Temperature", *Thin Solid Films*, **441**, 271-276 (2003).
- [7] A. Fujishima, T. N. Rao, and D. A. Tryk, "Titanium Dioxide Photocatalysis", *Journal of Photochemistry and Photobiology C: Photochemistry Reviews*, **1**, 1-21 (2000).
- [8] U. Diebold, "The Surface Science of Titanium Dioxide", *Surface Science Reports*, **48**, 53-229 (2003).
- [9] B. S. Richards, "Novel Uses of Titanium Dioxide for Silicon Solar Cells", PhD. Thesis. University Of New South Wales, April 2002.
- [10] *Kirk-Othmer Encyclopedia of Chemical Technology*, Metal and Alloys: Titanium and Titanium Alloys, F. H. (Sam) Froes, University Of Idaho. Article Online Posting Date (October 18, 2001), John Wiley & Sons, Inc, 2005. Web Address: <http://www.mrw.interscience.wiley.com/kirk>. Accessed on August 2005.
- [11] O. Carp, C.L. Huisman, and A. Reller, "Photoinduced Reactivity of Titanium Dioxide", *Progress in Solid State Chemistry*, **32**, 33-177 (2004).

- [12] Z.W. Zhao, B.K. Tay, S.P. Lau, and G.Q. Yu, "Optical Properties of Titania Films Prepared by Off-Plane Filtered Cathodic Vacuum Arc", *Journal of Crystal Growth*, **268**, 543-546 (2004).
- [13] A.P. Xagas, E. Androulaki, A. Hiska, and P. Falaras, "Preparation, Fractal Surface Morphology and Photocatalytic Properties of TiO₂ Films", *Thin Solid Films*, **357**, 173-178 (1999).
- [14] G. Cangiani, "AB-Initio Study of the Properties of TiO₂ Rutile and Anatase Polytypes", PhD. Thesis. Universite de Trieste, Italy. June 2003.
- [15] A. Fujishima, K. Hashimoto and T. Watanabe, "*TiO₂ photocatalysis: Fundamentals and Applications*", BKC INC, Tokyo, 2001.
- [16] C. Sittig, M. Textor, and N.D. Spencer, "Surface Characterization of Implant Materials c.p. Ti, Ti-6Al-7Nb and Ti-6Al-4V with Different Pre-Treatment", *Journal of Materials Science: Materials in Medicine*, **10**, 35-46 (1999)
- [17] X. Liu, P. K. Chu, and C. Ding, "Surface Modification of Titanium, Titanium Alloys, and Related Materials for Biomedical Applications." *Materials Science and Engineering Research*, **47**, 49-12 (2004).
- [18] J. Lindigkeit, "Titanium in Dentistry", pp. 453-466 in *Titanium and Titanium Alloys: Fundamentals and Applications*. Edited by C. Leyerns and M. Peters. Wiley-VCH Verlag GmbH & Co., Weinheim, 2003.
- [19] J. Barksdale, *Titanium: Its Occurrence, Chemistry and Technology*, The Ronald Press Company, New York, 1949.
- [20] G.V. Samsonov, *The Oxide Handbook*. IFI/Plenum Press, New York, 1982
- [21] A. D. Mc Quillan, and M. K. Mc Quillan, *Titanium*. Butterworths Scientific Publications, London, 1956.
- [22] X. Bokhimi, A. Morales, M. Aguilar, J.A. Toledo-Antonio and F. Pedraza, "Local Order in Titania Polymorphs", *International of Hydrogen Energy*, **26**, 1279-1287 (2001).
- [23] S. Matsuda, and A Kato, "Titanium Oxide Based Catalysis - A Review", *Applied Catalysis*, **8**, 149-165 (1983).
- [24] M.A. Afifi, M.M. Abdel-Aziz , I.S. Yahia, M. Fadel, L.A. Wahab, " Transport Properties of Polycrystalline TiO₂ and Ti₂O₃ as Semiconducting Oxides", *Journal of Alloys and Compounds*, **455**, (2008) 92-97

- [25] J. I. Murray and H.A. Wreidt, "Oxygen-Titanium", pp 1789-1794 in *Binary Alloys Phase Diagram, Volume 2*, Edited by T.b. Massalski, American Society for Metals, Metals Park, Ohio, 1987.
- [26] S. Anderson, B. Collen, U. Kuylenstierna, and A. Magneli, "Phase Analysis Studies on the Titanium-Oxygen System", *Acta Chem. Scand* **11**, 1641-1652 (1957)
- [27] H. Nowotny and E. Dimakopoulou, "Die Phase TiO₂", *Monatsh. Chem. (Germany)*, **90**, 620-622 (1959).
- [28] S. Yamaguchi, "Interstitial Order-Disorder Transformation in the Ti-O Solid Solution. I. Ordered Arrangement of Oxygen", *Journal of Physic Society Japan*, **27**[1], 155-163 (1969).
- [29] S. Yamaguchi, K. Hiraga and M. Hirabayashi, "Interstitial Order-Disorder Transformation in the Ti-O Solid Solution. IV. A Neutron Diffraction Study" *Journal of Physic Society Japan*, **28**, 1014-1023 (1970).
- [30] F.W. Vahldiek, "Phase Transition of Titanium Dioxide under Various Pressures", *Journal of Less-Common Metal*, **11**, 99-110 (1966).
- [31] F. Dacheille, P.Y. Simons, and R. Roy, "Pressure-Temperature Studies of Anatase, Brookite, Rutile and TiO₂-II", *American Mineralogist*, **53**, 1929-1939 (1968).
- [32] R. Roy and W.B. White, "Growth of Titanium Oxide Crystals of Controlled Stoichiometry and Order", *Journal of Crystal Growth*, **13-14**, 78-83 (1972).
- [33] J.M.G. Amores, U.C. Escribano, and G. Busca, "Anatase Crystal Growth and Phase Transformation to Rutile in High-Area TiO₂ MoO₃-TiO₂ and other TiO₂-supported Oxide Catalytic system", *Journal of Material Chemistry*, **5**, 1245-1249 (1995).
- [34] A. Bendavid, P.J. Martin, and H. Takikawa, "Deposition and Modification of Titanium Dioxide Thin Films by Filtered Arc Depositions", *Thin Solid Film*, **360**, 241-249 (2000).
- [35] M. Yokozawa, H. Iwasa, and I. Teramoto, "Vapor Deposition of TiO₂", *Japanese Journal of Applied Physics*, **7**, 96-97 (1968).
- [36] P. Löbl, M. Hupperta, and D. Mergel, "Nucleation and Growth in TiO₂ Films Prepared by Sputtering and Evaporation", *Thin Solid Films*, **251**, 72-79 (1994).
- [37] V.G. Erkov, S.F. Devyatova, E.L. Molodstova, T.V. Malsteva, and U.A. Yanovskii, "Si-TiO₂ Interface Evolution at Prolonged Annealing in Low Vacuum or N₂O Ambient", *Applied Surface Science*, **166**, 51-56 (2000).

- [38] B.E. Yoldas and D.P. Partlow, "Formation of Broad Band Reflective Coating on Fused Silica for High Power Laser Applications", *Thin Solid Films*, **129**, 1-4 (1985).
- [39] C.R. Ottermann and K. Bange, "Correlation between the Density of TiO₂ Films and Their Properties", *Thin Solid Films*, **286**, 32-34 (1996).
- [40] E.T. Fitzgibbons, K.J. Sladek and W.H. Hartwig, "TiO₂ Film Properties as a Function of Processing Temperature", *Journal of The Electrochemical Society*, **119**, 735-739 (1972).
- [41] G. Hass, "Preparation, Properties and Optical Applications of Thin Films of Titanium Dioxide", *Vacuum*, **11**, 331-345 (1952).
- [42] M.W. Ribarsky, "Titanium Dioxide (TiO₂) (Rutile)", pp 795-804 in *Handbook of Optical Constants, Vol. 1*. Edited by E. Palik. Academic Press Inc., Orlando, 1985.
- [43] Q. Liu, J. Ding, F.K. Mante, S.L. Wander, and G.R. Baran, "The Role of Surface Functional Groups in Calcium Phosphate Nucleation on Titanium Foil: A self-assembled Monolayer Technique", *Biomaterials*, **23**, 3103-3111 (2002).
- [44] R. J. Meyer and E.H.E. Pietsch, *Gmelins Handbuch Der Anorganischen Chemie: Titan. Vol. 41*. Verlag Chemie, Weinheim, 1951
- [45] H. Tang, H. Berger, P.E. Schmid, and F. Levy, "Optical Properties of Anatase TiO₂", *Solid State Communications*, **92**, 267-271 (1994).
- [46] W.D. Kingery, H.K. Bowen, and D.R. Uhlmann, *Introduction to Ceramics*. Wiley, New York, 1976.
- [47] E. W. Washburn, *International Critical Table of Numerical Data, Physics, Chemistry and Technology*. Mc-Graw Hill, New York, 1930.
- [48] S.Y. Kim, "Simultaneous Determination of Refractive Index, Extinction Coefficient, and Void Distribution of Titanium Dioxide Thin Film by Optical Methods", *Applied Optics*, **35**, 6703-6707 (1996).
- [49] C. Damm, F.W. Müller, G. Israel, S. Gablenz, and H.P. Abicht, "Structural Influences on the Photoelectric Properties of TiO₂", *Dyes and Pigments*, **56** 151-157 (2003).
- [50] R.I. Bickley, T. Gonzales-Carreno, S.J. Lees, L. Palmisano, and R.J. D.Tilley, "A Structural Investigation of Titanium Dioxide Photocatalysts", *Journal of Solid State Chemistry*, **92** [1] 178-190 (1991).

- [51] S.S. Watson, D. Beydoun, J.A. Scott, and R. Amal, "The Effect of Preparation Method on the Photoactivity of Crystalline Titanium Dioxide Particles", *Chemical Engineering Journal*, **95**, 213-220 (2003).
- [52] T. Ohno, K. Sarukawa, K. Tokieda, and M. Matsumura, "Morphology of a TiO₂ Photocatalyst (Degussa, P-25) Consisting of Anatase and Rutile Crystalline Phases", *Journal of Catalysis*, **203**, 82-86 (2001).
- [53] T. Ohno, K. Fujihara, K. Sarukawa, K. Tokieda, and M. Matsumura, "Splitting of Water by Combining Two Photocatalytic Reactions Through a Quinone Compound Dissolved in an Oil Phase", *Physical Chemistry*, **213**, 165-174 (1999).
- [54] R.W. Harold, "An Introduction to Appearance Analysis", *Second Sight*, [84] 1-7 (2001).
- [55] P. Vuvlstecker, 2004
[http://escience.anu.edu.au/lecture/cg/Color/HSV_HLS.en.html]. Accessed on 20th October 2008.
- [56] D.E.P. Hoy, "On the Use of Color Imaging in experimental", *Experimental Techniques*, **21**, 1997, p17-19.
- [57] V. Vezhnevets, V. Sazonov, and A. Andreeva, "A Survey on Pixel-Based Skin Color Detection Techniques", pp. 85-92 in Proceeding of International Conference on Computer Graphics & Vision (Graphicon), Moscow, 5-10 Sept (2003) <http://graphics.cs.msu.ru/en/publications/text/gc2003vsa.pdf>
- [58] P. Bourke, "HSL Colour Space" Edited at 2000
[http://ozviz.wasp.uwa.edu.au/~pbourke/texture_colour/convert/]. Accessed on 20th October 2008.
- [59] C. Poynton, "A Guide of Color Space, New Foundation for Video Technology", pp. 167-180 in Proceeding of the SMPTE Advanced Television and Electronic Imaging Conference, San Francisco, Feb. (1995).
- [60] F. Busby, K.R. Hughes, and K. Hyun, "Color Measurement Techniques for Rapid Determination of Residence Time Distribution", pp. 230-232 in Proceeding SPE/ANTEC 1999, New York City, May 2-6 (1999).
- [61] S.V. Gils, P. Mast, E. Stijns, and H. Terryn, "Colour Properties of Barrier Anodic Oxide Films on Aluminium and Titanium Studied with Total Reflectance and Spectroscopic Ellipsometry", *Surface & Coating Technology*, **185**, 303-310 (2004).

- [62] Y.T. Sul, C.B. Johanson, Y. Jeong, and T. Albrektsson, "The Electrochemical Oxide Growth Behaviour on Titanium in Acid and Alkaline Electrolytes", *Medical engineering Physics*, **23**, 329-346 (2001).
- [63] J.L. Delplancke, M. Degrez, A. Fontana, and R. Winand, "Self-Color Anodizing of Titanium", *Surface Technology* **16**, 153-162 (1982).
- [64] M.A. Iman, and A.C. Fraker, "Titanium Alloys as Implant Materials", pp. 3-16 in *Medical Applications of Titanium and Its Alloys: The Material and Biological Tissues*, ASTM STP 1272. Edited by S. A. Brown and J. E. Lemons. American Society for Testing and Materials, Ohio, 1996.
- [65] J.J. Polmear, *Titanium Alloys*. Edwards Arnold Publications, London, 1981.
- [66] P.J. Bania, "Titanium Alloys in The 1990's", pp. 3-14 in *The Mineral, Metals & Material Society*. Edited by D. Eylon, R.R. Boyer, and D.A. Koss. Warrendale, PA, 1993.
- [67] R.W. Schutz, "Beta Titanium Alloys in The 1990's", pp. 75-91 in *The Mineral, Metals & Material Society*. Edited by D. Eylon, R.R. Boyer, and D.A. Koss. Warrendale, PA, 1993.
- [68] P. Thomsen, C. Larsson, L.E. Ericson, L. Sennerby, J. Lausmaa, and B. Kasmö, "Structure of the interface between rabbit cortical bone and implants of gold, zirconium and titanium", *Journal of Materials Science: Materials in Medicine*, **8** [11], 653-665 (1997).
- [69] J. Breme, E. Eisenbarth, and V. Biehl, "Titanium and Its Alloys for Medical Applications", pp. 412-443 in *Titanium and Titanium Alloys: Fundamentals and Applications*. Edited by C. Leyerns and M. Peters. Wiley-VCH Verlag GmbH & Co. KGaA, Weinheim, 2003.
- [70] M. Peters, J. Kumpfert, C.H. Ward, and C. Leyerns, "Titanium Alloys for Aerospace Applications", pp. 333-350 in *Titanium and Titanium Alloys: Fundamentals and Applications*. Edited by C. Leyerns and M. Peters. Wiley-VCH Verlag GmbH & Co. KGaA, Weinheim, 2003.
- [71] M. Peters and C. Leyerns, "Non-Aerospace Applications of Titanium and Titanium Alloys", pp. 393-422 in *Titanium and Titanium Alloys: Fundamentals and Applications*. Edited by C. Leyerns and M. Peters. Wiley-VCH Verlag GmbH & Co. KGaA, Weinheim, 2003.
- [72] C.T. Hanks, J.C. Watahaz, and Z. Suni, "In Vitro Models of Biocompatibility: A Review." *Dental Materials*, **12**, 186-193 (1996).

- [73] T. Kokubo, H. Kushitani, S.S.T. Kitsugi, and T. Yamamum, "Solutions Able to Reproduce *In Vivo* Surface-Structure Changes in Bioactive Glass-Ceramic A-W3", *Journal of Biomedical Materials Research*, **24**, 721-734 (1990).
- [74] M.B. Pabbruwe, "The Effect of Bioceramics Chemistry on Cellular Behaviour *In Vitro* and Bone Formation *In Vivo*," PhD. Thesis, The University of New South Wales, February 2002.
- [75] G. Schmalz, "Agar Overlay Method", *International Endodontic Journal*, **21** 59-66 (1988).
- [76] H.M. Kim, T. Himeno, T. Kokubo, and T. Nakamura, "Process and Kinetics of Bonelike Apatite Formation on Sintered Hydroxyapatite in a Simulated Body Fluid." *Biomaterials*, **26**, 4366-4373 (2005).
- [77] X. Lu, and Y. Leng, "Theoretical Analysis of Calcium Phosphate Precipitation in Simulated Body Fluid." *Biomaterials*, **26**, 1097-1108 (2005).
- [78] A. Oyane, K. Onuma, I. Atsuo, H.M. Kim, T. Kokubo, and T. Nakamura, "Formation and Growth of Clusters in Conventional and New Kinds of Simulated Body Fluid", *Journal of Biomedical Materials Research A*, **64**, 339-348 (2003).
- [79] T. Himeno, M. Kawashita, H.M. Kim, T. Kokubo, and T. Nakamura, "Zeta-Potential Variation of Bioactive Titanium Metal During Apatite Formation on its Surface in Simulated Body Fluid." pp. 641-644 in *Bioceramics*. Edited by S.Brown, I. R. Clarke, and P.Williams. Trans Tech Publishers, Switzerland, 2001.
- [80] M.S. Tung, *Calcium phosphate in biological and industrial system*. Kluwer Academic Publishers, Dordrecht, 1998.
- [81] M. Ahmad, D. Gawronski, J. Blum, J. Goldberg, and G. Gronowicz, "Differential Response of Human Osteoblast-like Cells to Commercially Pure (cp) Titanium Grades 1 and 4", *Journal of Biomedical Research*, **46**, 121-131 (1999).
- [82] I. Degasne, M.F. Baslé, V. Demais, G. Huré, M. Lesourd, B. Grolleau, L. Mercier, and D. Chappard, "Effects of Roughness, Fibronectin and Vitronectin on Attachment, Spreading, and Proliferation of Human Osteoblast-Like Cells (Saos-2) on Titanium Surfaces", *Calcified Tissue International*, **64**, 499-507 (1999).
- [83] X. Zhu, J. Chen, L. Scheideler, R. Reichl, and J. Geis-Gerstorfer, "Effects of Topography and Composition of Titanium Surface Oxides on Ostoeblast Responses", *Biomaterials*, **25**, 4087-4103 (2004).

- [84] J. Fogh, J.M. Fogh, and T. Orfeo, "One Hundred and Twenty-Seven Cultured Human Tumor Cell Lines Producing Tumors in Nude Mice", *Journal of The National Cancer Institute*, **59**, 221–226 (1977).
- [85] S.B. Rodan, Y. Imai, M.A. Thiede, G. Wesolowski, D. Thompson, Z. Bar-Shavit, S. Shull, K. Mann, and G.A. Rodan, "Characterisation of a Human Osteosarcoma Cell Line (Saos-2) with Osteoblastic Properties", *Cancer Research*, **47**, 4961-4966 (1987).
- [86] A. Okumura, M. Goto, T. Goto, M. Yoshinari, S. Masuko, T. Katsuki, and T. Tanaka, "Substrate Affects the Initial Attachment and Subsequent Behavior of Human Osteoblastic cells (Saos-2)", *Biomaterials*, **22**, 2263-2271 (2001).
- [87] R. Rajaraman, D.E. Rounds, S.P.S. Yen, and A. Rembaum, "A Scanning Electron Microscope Study of Cell Adhesion and Spreading In-Vitro", *Experimental Cell Research*, **88**, 327-339 (1974).
- [88] K. Das, S. Bose, and A. Bandyopadhyay, "Surface Modifications and Cell-Materials Interactions with Anodized Ti", *Acta Biomaterialia*, **3**, 573-585 (2007).
- [89] P-I. Branemark, "Osseointegration and its Experimental Background", *The Journal of Prosthetic Dentistry*, **50**, 399-410 (1983).
- [90] H.M. Kim, F. Miyaji, T. Kokubo, and T. Nakamura, "Preparation of Bioactive Ti and its Alloys via Simple Chemical Surface Treatment." *Journal of Medical Materials Research*, **32**, 409-417 (1996).
- [91] H.M. Kim, F. Miyaji, and T. Kokubo, "Effect of Heat Treatment on Apatite-Forming Ability of Ti Metal Induced by Alkali Treatment", *Journal of Materials Science: Materials in Medicine*, **8**, 341-347 (1997).
- [92] M.F. Maitz, M.T. Pham, W. Matz, H. Reuther, G. Steiner, and E. Richter, "Ion Beam Treatment of Titanium Surfaces for Enhancing Deposition of Hydroxyapatite from Solution", *Biomolecular Engineering*, **19**, 269-272 (2002).
- [93] K.T. Bowers, J.C. Keller, B.A. Randolph, D.G. wick, C.M. Michaels, "Optimization of Surface Micromorphology for Enhanced Osteoblast Responses In-Vitro", *International Journal of Oral Maxillofacial Implants*, **7**, 302-310 (1992).
- [94] A. Letic-Gavrilovic, R. Scandurra, K. Abe, "Genetic Potential of Interfacial Guided Osteogenesis in Implant Devices", *Dentistry Materials Journal*, **19**, 99-132 (2000).

- [95] J.Y. Martin, Z. Schwartz, T.W. Hummert, D.M. Schraub, J. Simpson, J. Lankford, D.D. Dean, D.L. Cochran, and B.D. Boyan, "Effect of Titanium Surface Roughness on Poliferation, Differentiation, and Protein Synthesis of human osteoblast-like cells (MG63)", *Journal of Biomedical Materials Research*, **29**, 389-401 (1995).
- [96] D.E., Mac Donald, N. Deo, B. Markovic, M. Stranick, and P. Somasundaran "Adsorption and Dissolution Behavior of Human Plasma Fibronectin on Thermally and Chemically Modified Titanium Dioxide Particles", *Biomaterials*, **23**, 1269-1279 (2002).
- [97] T. Hanawa, "In Vivo Metallic Biomaterials and Surface Modification", *Materials Science and Engineering Research A*, **27**, 260-266 (1999).
- [98] R.L. Williams, S.A. Brown, and K. Merritt, "Electrochemical Studies on the Influence of Protein on the Corrosion of Implant Alloys", *Biomaterials*, **9**, 181-186 (1988).
- [99] D.F. Williams, *Biocompatibility of Clinical Implant Materials*. CRC Press, Bota Raton, FL, 1981.
- [100] K. Hayashi, I. Noda, K. Uenogama, and Y. Sugioka, "Breakdown Corrosion Potential of Ceramic Coated Metal Implants", *Journal of Biomedical Materials Research*, **24**, 1111-1113 (1990).
- [101] J.E. Sundgren, P. Bodo, and I. Lundstrom, "Auger Electron Spectroscopic Studies of the Interface between Human Tissue and Implants of Titanium and Stainless Steel", *Journal of Colloid and Interface Science*, **110**, 9-20 (1986).
- [102] M.P. Moret, R. Zallen, D.P. Vjay, and S.B. Desu, "Brookite-Rich Titania Films Made by Pulsed Laser Deposition", *Thin Solid Films*, **366**, 8-10 (2000).
- [103] W.H. Song, Y.K. Jun, Y. Han, and S.H. Hong, "Biomimetic Apatite Coatings on Micro-Arc Oxidized Titania", *Biomaterials*, **25**, 3341-3349 (2004).
- [104] H.J. Oh, J.H. Lee, Y. Jeong, Y.J. Kim, and C.S. Chi, "Microstructural Characterization of Biomedical Titanium Oxide Film Fabricated by Electrochemical Method", *Surface & Coatings Technology*, **198**, 247-252 (2005).
- [105] V. Guidi, M.C. Carotta, M. Ferroni, G. Martinelli, L. Paglialonga, E. Comini, and G. Sberveglieri, "Preparation of Nanosized Titania Thick and Thin Films as Gas-Sensors", *Sensors and Actuators B*, **57**, 197-200 (1999).

- [106] C. Kaya, F. Kaya, B.T.B. Suc, and A.R Boccaccini, “Structural and Functional Thick Ceramic Coatings by Electrophoretic Deposition”, *Surface & Coatings Technology*, **191**, 303- 310 (2005).
- [107] N. Ogata, J.V. Tassel, and C.A Randall, “Electrode Formation by Electrophoretic Deposition of Nanopowders”, *Materials Letters*, **49**, 7-14 (2001).
- [108] F. Tang, T. Uchikoshi, T. S. Suzuki, and Y. Sakka, “Alignment of TiO₂ Particles by Electrophoretic Deposition in a High Magnetic Field”, *Materials Research Bulletin*, **39**, 2155-2161 (2004).
- [109] M. Textor, C. Sittig, V. Frauchiger, S. Tosatti, and D.M. Brunette, *Titanium in Medicine*, Springer, Berlin, 2001.
- [110] I.S. Park, T.G. Woo, M.H. Lee, S.G. Ahn, M.S. Park, T.S. Bae, and K.W. Seol, “Effects of Anodizing Voltage on The Anodized and Hydrothermally Treated Titanium Surface”, *Metals and Materials International*, **12**, 505-511 (2006).
- [111] B. Yang, M. Uchida, H.M. Kim, X. Zhang, and T. Kokubo, “Preparation of Bioactive Titanium Metal via Anodic Oxidation Treatment”, *Biomaterials*, **25**, 1003-1010 (2004).
- [112] H.Z. Abdullah and C.C. Sorrell, “Preparation and Characterisation of TiO₂ Thick Films Fabricated by Anodic Oxidation”, *Materials Science Forum*, **561-565**, 2159-2162 (2007).
- [113] S. Ikonopisov, “Theory of Electrical Breakdown During Formation of Barrier Anodic Films”, *Electrochimica Acta*, **22**, 1077-1082 (1977).
- [114] I. Montero, M. Fernandez, and J.M. Albella, “Pore Formation During The Breakdown Process in Anodic Ta₂O₅ Films”, *Electrochimica Acta*, **32**, 171-174 (1987).
- [115] A.L. Yerokhin, X. Nie, A. Leyland, A. Matthews, and S.J. Dowey, “Plasma Electrolysis for Surface Engineering”, *Surface and Coatings Technology*, **122**, 73-79 (1999).
- [116] D. Capek, M.-P. Gigandet, M. Masmoudi, M. Wery, and O. Banakh, “Long-Time Anodisation of Titanium in Sulphuric Acid”, *Surface and Coating Technology*, **202**, 1379-1384 (2008).
- [117] M.V. Diamanti, and M.P. Pedferri, ‘Effect of Anodic Oxidation Parameters on the Titanium Oxides Formation’, *Corrosion Science*, **49**, 939-948 (2007).

- [118] B. Liang, S. Fujibayashi, J. Tamura, M. Noe, H.M. Kim, M. Uchida, T. Kokubo, and T. Nakamura, "Bone-Bonding Ability of Anodic Oxidized Titanium". Editors: B. Ben-Nissan, D. Sher, and W. Walsh, *Bioceramics*, **15**, (Trans Tech Publishers, Switzerland), 923-926 (2002).
- [119] M.L. Hitchman, R.A. Spackman, and C. Agra, "Photoelectrochemical Study of Titanium Dioxide Films Prepared by Anodisation of Titanium Metal in Sulfuric Acid", *Journal of Chemical Society: Faraday Transaction*, **92**, 4049-4052 (1996).
- [120] C.H. Kim, S.I. Pyun, and E.J. Lee, "Donor Distribution over Anodically Passivating Crystalline and Amorphous TiO₂ Films", *Materials Letters*, **10**, 387-391 (1991).
- [121] J.P. Gueneau de Mussy, G. Langelaan, J. Decerf, and J.L. Delplancke, "TEM and X-Ray Diffraction Investigation of The Structural Characteristics of the Microporous Oxide Film Formed on Polycrystalline Ti", *Scripta Materialia*, **48**, 23-29 (2003).
- [122] C. Jaeggi, P. Kern, J. Michler, J. Patscheider, J. Tharian, and F. Munnik, "Film Formation and Characterization of Anodic Oxides on Titanium for Biomedical Applications", *Surface and Interface Analysis*, **38**, 182-185 (2006).
- [123] T.Y. Xiong, X.Y. Cui, H.M. Kim, M. Kawashita, T. kokubo, J. Wu, H.-Z. Jin, and T. Nakamura, "Effect of Surface Morphology and Crystal Structure on Bioactivity of Titania Films Formed on Titanium Metal via Anodic Oxidation in Sulfuric Acid Solution", *Key Engineering Materials*, **254-256**, 375-378 (2004).
- [124] P. Tengvall, H. Elwing, L. Sjöqvist, I. Lundström, and L.M. Bjursten, "Interaction between Hydrogen Peroxide and Titanium: A Possible Role in the Biocompatibility of Titanium", *Biomaterials*, **10**, 118-120 (1989a).
- [125] P. Tengvall, I. Lundström, L. Sjöqvist, H. Elwing, and L.M. Bjursten, "Titanium-Hydrogen Peroxide Interaction: Model Studies of the Influence of the Inflammatory Response on Titanium Implants", *Biomaterials*, **10**, 166-175 (1989b).
- [126] J.H. Yi, C. Bernard, F. Variola, S.F. Zalzal, J.D. Wuest, F. Rosei, and A. Nanci, "Characterization of a Bioactive Nanotextured Surface Created by Controlled Chemical Oxidation of Titanium", *Surface Science*, **600**, 4613-4621 (2006).
- [127] X.X. Wang, S. Hayakawa, K. Tsuru, and A. Osaka, "Bioactive Titania Gel Layers Formed by Chemical Treatment of Ti Substrate with a H₂O₂/HCl Solution", *Biomaterials*, **23**, 1353-1357 (2002).

- [128] J.M. Wu, S. Hayakawa, K. Tsuru, and A. Osaka, "Porous Titania Films Prepared from Interactions of Titanium with Hydrogen Solution", *Scripta Materialia*, **46**, 101-106 (2002).
- [129] A. Afshar and M.R. Vaezi, "Evaluation of Electrical Breakdown of Anodic Films on Titanium in Phosphate-Base Solutions", *Surface and Coatings Technology*, **186**, 398-404 (2004).
- [130] S.J. Park, "Chemical Observation of Anodic TiO₂ for Biomaterial Application", *Metals and Materials International*, **14**, 449-455 (2008).
- [131] N.K. Kuromoto, R.A. Simão, and G.A. Soares, "Titanium Oxide Films Produced on Commercially Pure Titanium by Anodic Oxidation with Different Voltages", *Materials Characterization*, **58**, 114-121 (2007).
- [132] V.M. Frauchiger, F. Schlottig, B. Gasser, and M. Textor, "Anodic Plasma-Chemical Treatment of CP Titanium Surfaces for Biomedical Applications", *Biomaterials*, **25**, 593-606 (2004).
- [133] I.S. Park, M.H. Lee, T.S. Bae, and K.W. Seol, "Effects of Anodic Oxidation Parameters on a Modified Titanium Surface", *Journal of Biomedical Research Part B: Applied Biomaterials*, **84B**, 422-42 (2008).
- [134] Y. Han, S.H. Hong, and K. Xu, "Structure and In Vitro Bioactivity of Titania-Based Films by Micro-Arc Oxidation", *Surface and Coatings Technology*, **168**, 249-258 (2003).
- [135] H. Ishizawa and M. Ogino, "Characterization of Thin Hydroxyapatite Layers Formed on Anodic Titanium Oxide Films Containing Ca and P by Hydrothermal Treatment", *Journal of Biomedical Materials Research*, **29**, 1071-1079 (1995).
- [136] H. Ishizawa and M. Ogino, "Formation and Characterization of Anodic Titanium Oxide Films Containing Ca and P", *Journal of Biomedical Materials Research*, **29**, 65-72 (1995).
- [137] D. Buser, R.K. Schenk, S. Steinmann, J.P. Fiorellini, C.H. Fox, and H. Stich, "Influence of Surface Characteristics on Bone Integration of Titanium Implants. A Histomorphometric Study in Miniature Pigs", *Journal of Biomedical Materials Research*, **25**, 889-902 (1991).
- [138] A. Nanci, J.D. Wuest, L. Peru, P. Brunet, V. Sharma, S. Zalzal, and M. D. McKee, "Chemical Modification of Titanium Surfaces for Covalent Attachment of Biological Molecules", *Journal of Biomedical Materials Research*, **40**, 324-335 (1998).

- [139] M. Takeuchi, Y. Abe, Y. Yoshida, Y. Nakayama, M. Okazaki, and Y. Akagawa, "Acid Pretreatment of Titanium Implants", *Biomaterials*, **24**, 1821-1827 (2003).
- [140] H.B. Wen, J.G.C. Wolke, J.R. Wijn, Q.F.Z.C. Liu, and K. de Groot, "Fast Precipitation of Calcium Phosphate Layers on Titanium Induced by Simple Chemical Treatments", *Biomaterials*, **18**, 1471-1478 (1997).
- [141] Y. Han and K. Xu, Photoexcited Formation of Bone Apatite-Like Coatings on Micro-Arc oxidized Titanium, *Journal of Biomedical Materials Research A*, **71**, 608-614 (2004).
- [142] L. Jonášová, F.A. Müller, A. Helebrant, J. Strnad, and P. Greil, "Biomimetic Apatite Formation on Chemically Treated Titanium", *Biomaterials*, **25**, 1187-1194 (2004).
- [143] F.J. Gil, A. Padro's, J.M. Manero, C. Aparicio, M. Nilsson, and J.A. Planell, "Growth of Bioactive Surfaces on Titanium and its Alloys for Orthopaedic and Dental Implants", *Materials Science and Engineering Research C*, **22**, 53-60 (2002).
- [144] H.Z. Abdullah and C.C. Sorrell, "Anodic Oxidation of Titanium", *Materials Australia*, **41**, 44-46 (2008).
- [145] T. Kokubo and H. Takadama, "How Useful is SBF in Predicting *In Vivo* Bone Bioactivity?", *Biomaterials*, **27**, 2907- 2919 (2006).
- [146] Web address: <http://www.colorpro.com/info/tools/convert.htm>. CEI Flow Master Products LLC, Hudson USA (2007). Accessed on 28th November 2008.
- [147] NanoCalc Manual, version 2.31, (2005), Mikropack GmbH, Germany
- [148] American Society for Testing and Materials, ASTM (C 1624-05), *Standard Test Method for Adhesion Strength and Mechanical Failure Modes of Ceramic Coating by Quantitative Single Point Scratch Testing*.
- [149] V. Jantou, D.S. McPhail, R.J. Chater, and A. Kearsly, "Analysis of Simulated Hypervelocity Impact on a Titanium Fuel Tank from the Salyut 7 Space Station", *Applied Surface Science*, **252**, 7120-7123 (2006).
- [150] C.E.B. Marino, P.A.P. Nascente, S.R. Biaggio, R.C. Rocha-Filho, and N. Bocchi, "XPS Characterization of Anodic Titanium Oxide Films Grown in Phosphate Buffer Solution", *Thin Solid Films*, **468**, 109-112 (2004).

- [151] Y.T. Sul, C.B. Johansson, S. Petronis, A. Krozer, Y. Jeong, A. Wennerberg, T. Albrektsson, "Characteristics of the Surface Oxides on Turned and Electrochemically Oxidized Pure Titanium Implants up to Dielectric Breakdown: The Oxide Thickness, Micropore Configurations, Surface Roughness, Crystal Structure and Chemical Composition", *Biomaterials*, **23**, 491-501 (2002).
- [152] D.J. Blackwood, L.M. Petter, "The Influence of Growth rate on the Properties of Anodic Oxide Films on Titanium", *Electrochim Acta*, **34**, 1505-1511 (1989).
- [153] K. Nakano, K. Matsuo, K. Tomono, and N. Nakahara, "Sol and Gel Formation in Reaction of Amorphous Titania with H₂O₂ and HNO₃", *Corrosion Science*, **31**, 407-412 (1990).
- [154] M.V. Diamanti, B.D. Curto, and M.P. Pedferri, "Interference Colors of Thin Oxide Layers on Titanium", *Color Research and Application*, **33**, 221-228 (2008).
- [155] C. Jaeggi, P. Kern, J. Michler, T. Zehnder, and H. Siegenthaler, "Anodic Thin Films on Titanium used as Masks for Surface Micropatterning on Biomedical Devices", *Surface and Coating Technology*, **200**, 1913-1919 (2005).
- [156] X.Y. Li, and S. Taniguchi, "Oxidation Behavior of TiAl Based Alloys in a Simulated Combustion Atmosphere", *Intermetallic*, **12**, 11-12 (2004).
- [157] D.D. Deligianni, N.D. Katsala, P.G. Koutsoukos, and Y.F. Missirlis. "Effect of Surface Roughness of Hydroxyapatite on Human Bone Marrow Cell Adhesion, Proliferation, Differentiation and Detachment Strength", *Biomaterials*, **22**, 87-96 (2001).
- [158] J. Bico, U. Thiele, and D. Quéré, "Wetting of Textured Surfaces", *Colloids and Surfaces A: Physicochemical and Engineering Aspects*, **206**, 41-46 (2002)
- [159] P. Kern, P. Schwaller, and J. Michler, "Electrolytic Deposition of Titania Films as Interference Coatings on Biomedical Implants: Microstructure, Chemistry and Nano-Mechanical Properties", *Thin Solid Films*, **494**, 279-286 (2005).
- [160] A.B. Zuruzi, and N.C. MacDonald, "Facile Fabrication and Intergration of Patterned Nanostructured TiO₂ for Microsystems Applications", *Advanced Functional Materials*, **15**, 396-402 (2005).
- [161] T.H. Teh, A. Berkani, S. Mato, P. Skeldon, G.E. Thompson, H. Habazaki, and K. Shimizu, "Initial Stages of Plasma Electrolytic Oxidation of Titanium", *Corrosion Science*, **45**, 2757-2768 (2003).

- [162] J.C. Raposo, O. Zuloaga, M.A. Olazabal, J. M. Madariaga. “Development of a Modified Bromley Methodology for the Estimation of Ionic Media Effects on Solution Equilibria Part 6. The Chemical Model of Phosphoric Acid in Aqueous Solution at 25°C and Comparison with Arsenic Acid”, *Fluid Phase Equilibria*, **207**, 60-80 (2003).
- [163] A.R. Piggott, H. Leckie and L.L. Shreir, “Anodic Polarization of Ti in Formic Acid Anodic Behaviour of Ti in Relation to Anodizing Condition. *Corrosion Science*, **5** 165-184(1965).
- [164] J. Xu, C. Jia, B. Cao, and W.F. Zhang, “Electrochemical Properties of Anatase TiO₂ Nanotubes as an Anode Material for Lithium-Ion Batteries”, *Electrochimica Acta*, **52**, 8044-8047(2007)
- [165] E. Krasicka-Cydzik, “Gel-Like Layer Development During Formation of Thin Anodic Films on Titanium in Phosphoric Acid Solutions”, *Corrosion Science*, **46**, 2487-2502 (2004)
- [166] H. Habazaki, M. Uozumi, H. Konno, K. Shimizu, P. Skeldon, G.E. Thompson, “Crystalline of Anodic Titania on Titanium and Its Alloys”, *Corrosion Science*, **45**, 2063-2073 (2003)
- [167] J.H. Lee, S.E. Kim, Y.J. Kim, C.S. Chi, and H.J. Oh, “Effects of Microstructure of Anodic Titania on The Formation of Bioactive Compounds”, *Materials Chemistry and Physics*, **98**, 39-43 (2006)
- [168] P. Li, C. Ohtsuki, T. Kokubo, K. Nakanishi, N. Soga, and K. de Groot. “The Role of Hydrated Silica, Titania, and Alumina in Inducing Apatite on Implants”, *J. Biomed. Mater. Res.*, Vol. [28], (1994), 7-15.
- [169] T. Kasuga, H. Kondo, and M. Nogami, “Apatite Formation on TiO₂ in Simulated Body Fluid”, *Journal of Crystal Growth*, **235**, 235-240 (2002)
- [170] A. Aladjem, ‘Anodic Oxidation of Titanium and Its Alloy’, *Journal of Materials Science*, **8**, 688-704 (1973).
- [171] Y. Han, S.-H. Hong, and K.W. Xu, ‘Porous Nanocrystalline Titania Films by Plasma Electrolytic Oxidation’, *Surface and Coating Technology*, **154**, 314-318 (2002).
- [172] M.T. Pham, W. Matz, H. Reuther, E. Richter, G. Steiner, and S. Oswald, “Ion Beam Sensitizing of Titanium Surfaces to Hydroxyapatite Formation”, *Surfaces and Coating Technology*, **128-129**, 313-319 (2000).

- [173] L.H. Li, Y.M. Kong, H.W. Kim, H.E. Kim, S.J. Heo, and J.Y. Koak, "Improved Biological Performance of Titanium Implants due to Surface Modification by Micro-Arc Oxidation", *Biomaterials*, **25**, 2867-2875 (2004).
- [174] T. Kitsugi, T. Nakamura, M. Oka, Y. Senaha, T. Goto, and T. Shibuya, "Bone-bonding Behaviour of Plasma-Sprayed Coating of Bioglass, AW-Glass Ceramic, and Tricalcium Phosphate on Titanium Alloy", *Journal of Biomedical Materials Research*, **30**, 261-269 (1996).
- [175] H.Z. Abdullah and C.C. Sorrell, "TiO₂ Coating by Gel Oxidation", *Journal of Australia Ceramic Society*, In Press.
- [176] F. Liang, L. Zhou, and K. Wang, "Apatite Formation on porous Titanium by Alkali and Heat Treatment", *Surfaces & Coating Technology*, **165**, 133-139 (2003).
- [177] H.-M. Kim, F. Miyaji, T. Kokubo, S. Nishiguchi, T. Nakamura, "Graded Surface Structure of Bioactive Titanium Prepared by Chemical Treatment", *Journal of Biomedical Materials Research*, **45**, 100-107 (1996).
- [178] A. Nishikawa, *Technology of Monolithic Refractories*, Plibrico Japan Company Limited, Tokyo, 1984.
- [179] C.L. Chu, C.Y. Chung, J. Zhou, Y.P. Pu, and P.H. Lin, "Fabrication and Characterisation of Bioactive Sodium Titanate/Titania Graded Film on NiTi Shape Memory Alloy", *Journal of Biomedical Materials Research A*, **75**, 595-602 (2005).
- [180] U. Balachandran and N.G. Erov, "Raman Spectra of Titanium Dioxide", *Journal of Solid State Chemistry*, **42** 276-282 (1982).
- [181] J.C. Parker and R.W. Siegel, "Calibration of the Raman Spectrum to the Oxygen Stoichiometry of Nanophase TiO₂", *Applied Physics Letter*, **57** 943-945 (1990).
- [182] T. Ohsaka, F. Izumi, and Y. Fujiki, "Raman Spectrum of Anatase, TiO₂", *Journal of Raman Spectromicroscopy*, **7** 321-324 (1978).
- [183] B. Karunagaran, R.T.R. Kumar, V.S. Kumar, D. Mangalaraj, S.K. Narayandass, and G.M. Rao, "Structural; Characterisation of DC Magnetron-Sputtered TiO₂ Thin Film Using XRD and Raman Scattering Studies", *Materials Science Semiconductor Proc.* **6**, 547-550 (2003).